TECHNICAL MEMORANDUM

801

Implementation of a CAMS-based aerosol climatology in the IFS

A. Bozzo, S. Remy[1], A. Benedetti, J. Flemming, P. Bechtold, M.J. Rodwell and J.-J. Morcrette

Research Department

[1]LMD, IPSL, UPMC-CNRS, Paris

April 2017

European Centre for Medium-Range Weather Forecasts
Europäisches Zentrum für mittelfristige Wettervorhersage
Centre européen pour les prévisions météorologiques à moyen terme

Series: ECMWF Technical Memoranda

A full list of ECMWF Publications can be found on our web site under:
http://www.ecmwf.int/en/research/publications

Contact: library@ecmwf.int

European Centre for Medium-Range Weather Forecasts
Shinfield Park, Reading, RG2 9AX, England

Abstract

This document describes an aerosol climatology based on a set of reanalysis of atmospheric composition developed by Copernicus Atmosphere Monitoring Service (CAMS) and its implementation in the ECMWF Integrated Forecasting System (IFS). We discuss the technical aspects of the implementation and the impact of the new climatology on the model climate and on the medium-range weather forecasts.

CAMS provides operational daily analysis and forecast of aerosol optical depth (AOD) for five aerosol species using an on-line integrated module for aerosol and chemistry coupled to IFS (C-IFS). A fully prognostic aerosol model has a large impact on the weather forecasts in case of large aerosol concentrations as found during dust storms or strong pollution events. Due to its computational burden, prognostic aerosols are not yet feasible in the ECMWF operational weather forecasts though, and monthly-mean climatological fields are used instead.

We revised the aerosol climatology used in the operational ECMWF forecast model with one derived combining a set of short range forecasts and reanalysis for the period 2003-2014 with the CAMS system. The new climatology differs from the previous one both in the spatial distribution of the total AOD and the optical properties of each aerosol species. These changes affect the model mean biases at various spatial and temporal scales.

We report that the change to the new aerosol climatology has small a impact on the forecast skill of large-scale weather patterns but details of the regional distribution of aerosol radiative forcing can have a large local impact. This is the case of the area of the Arabian peninsula and the northern Indian Ocean where changes in the radiative forcing of the mineral dust significantly affect the summer monsoon circulation.

1 Introduction

Aerosols are among the major players in the radiative budget of the Earth-Atmosphere system. They participate in the atmospheric radiative transfer directly by scattering and absorbing electromagnetic radiation and indirectly by interacting with cloud microphysics (e.g. Haywood and Boucher, 2000; Bellouin et al., 2005). The uncertainty in the total radiative forcing by natural and anthropogenic aerosols remains large (Boucher et al., 2013) and most recent global climate models include more or less sophisticated prognostic aerosol schemes to explicitly take into account the direct radiative impact of aerosols on radiation and their interaction with cloud microphysics and other components of the Earth system (e.g. Bellouin et al., 2011; Donner et al., 2011; Stier et al., 2005). The impact of aerosols on the skill of numerical weather forecasting (NWP) models is less clear (Mulcahy et al., 2014) and conclusions vary depending on the diagnostics used (Reale et al., 2011) and on the spatio-temporal scales analysed (e.g. Rémy et al., 2015). Global and regional NWP models employ often an approximate treatment of aerosol radiative forcing based on a climatological description of their spatial distribution. This choice is due in part to the difficulty of assimilating real time observations to constrain the initialization of the prognostic aerosol field and in part to the fact that some species require an accurate prediction of their sources as for example in case of anthropogenic and natural fires. Moreover, coupling an NWP to an atmospheric composition model with a number (usually O(10)) of prognostic variable increases significantly the computational burden of the system but it might not translate directly into a clear improvement of the forecast skill (Morcrette et al., 2011; Mulcahy et al., 2014). Rodwell and Jung (2008) showed that a realistic representation of the mean climatological distribution of the most important aerosol species can already improve the forecast skill both on a regional scale and globally.

With a larger availability of computer resources and the improvement of chemical transport models, an increasing number of studies explored the impact of including various levels of complexity in the

representation of aerosol radiative effect in NWP models. Mulcahy et al. (2014) concluded that including both direct and first indirect radiative effects of prognostic aerosols in a global NWP model results mainly in a reduction in radiation and temperature biases on regional scale, with limited impact on weather forecast skill and a large uncertainty linked to the representation of the aerosol-clouds interaction. On the other hand, environmental products such as air quality forecasts greatly benefit from a complex aerosol scheme.

A prognostic aerosols scheme coupled to an NWP model has the largest impact on weather forecast skill for events associated with large aerosol optical depths such as dust storms. In these situations a realistic representation of the aerosol distribution can improve forecasts locally, especially close to the surface, and the direct dust aerosol radiative forcing feedbacks on the production of the aerosol itself (Rémy et al., 2015). Similarly, Toll et al. (2015) showed that capturing the distribution of aerosols during extreme fires events has a significant impact on near-surface weather forecasts for the affected areas.

In the operational configuration of the ECMWF Integrated Forecasting System (IFS) the aerosol direct radiative effect has always been treated using climatological aerosol distributions with no attempts in representing the interaction between aerosols and cloud microphysics. The current monthly-mean climatology of five main aerosol species ("OPER climatology" in the following) is based on one of the first multi aerosol model simulations by Tegen et al. (1997) and was implemented in 2003 substituting an earlier simpler annual mean distribution based on Tanré et al. (1984). When this more detailed climatology was introduced, it improved the model forecast skills mainly on a regional scale but, thanks to tele-connection feedbacks, it also affected the large scale mean flow (Rodwell and Jung, 2008). The tropical regions and in particular the monsoon areas of Western Africa and India showed the largest sensitivity to the change in aerosol radiative forcing, resulting in improvements in the precipitation bias (Tompkins et al., 2005).

Prognostic aerosols were introduced in the IFS for the first time with the GEMS project in 2005 (Hollingsworth et al., 2008) as part of the development of a real-time operational assimilation and forecast capability for aerosols, greenhouse and reactive gases. The aerosol assimilation and forecast model (Morcrette et al., 2009; Benedetti et al., 2009) has been further refined in the subsequent MACC projects (Simmons, 2010) and it is now maintained and developed within the Copernicus Atmosphere Monitoring Service (CAMS) as a suite of on-line integrated modules for aerosol and chemistry in IFS (C-IFS, Flemming et al., 2015). Morcrette et al. (2011) used an early version of C-IFS to explore the impact of coupled prognostic aerosol radiative effects on the quality of the operational IFS forecasts. They found that compared to the OPER climatology, the changes in medium-range large-scale forecast skill caused by having the prognostic aerosols interacting with radiation and cloud microphysics were small, although near-surface parameters showed local improvements. The inclusion of the full prognostic aerosol model had a prohibitive impact on the efficiency of the IFS, increasing the whole computational cost of the model by more than 50%.

Therefore a climatological description of aerosol distribution is still a viable option to capture the monthly-mean aerosol radiative effect for a NWP model (Toll et al., 2016). Improvements in aerosol climatologies are tied to improvement in chemical transport models and observations. A climatology can be built with a strong emphasis on surface observations using model fields to fill the gaps between the sparse network of measurement sites (e.g. Kinne et al., 2013), or merging model fields, satellite data and surface observations using empirical methods (e.g. Liu et al., 2005) or data assimilation system. The MACC Reanalysis of reactive trace gases and aerosols (MACCRA, Inness et al., 2013) was the first multi-year atmospheric composition reanalysis effort developed with the MACC system taking advantage of the 4-D variational assimilation system for atmospheric composition (Benedetti et al., 2009). Total aerosol optical depth (AOD) was constrained by assimilating the AOD retrieved from the Moderate resolution Imaging Spectroradiometer (MODIS) observations. CAMS will update MACCRA with a new high-resolution atmo-

spheric composition reanalysis in the next years but as an interim product between MACCRA and CAMS reanalysis, a new dataset (CAMSiRA, Flemming et al., 2017) was recently produced using the most up-to-date version of C-IFS. CAMSiRA shows a good agreement with the latest surface AOD observations, combines the most recent advances in global aerosol modelling and satellite retrieval and so it represents an improvement with respect to the current OPER climatology. It also provides a better framework to evaluate the impact of coupling the C-IFS prognostic aerosol model to the operational forecast system.

This documents describes the development of an aerosol monthly-mean climatology based on CAMSiRA (section 2) and its implementation in the operational IFS. We discuss the impact that the new climatology has on the mean climate of the IFS (section 3) and on its forecast skills (section 4 and 5). Finally we discuss the implication of our findings in the representation of aerosols in a global forecasting system and future work which could further improve how aerosols are treated in the IFS.

2 CAMS aerosol climatology

The aerosol model implemented in the CAMS system is based on the model developed at the Laboratoire d'Optique Atmospherique (LOA) Laboratoire de Meteorologie Dynamique (LMD) (Boucher et al., 2002; Reddy et al., 2005) with modifications by ECMWF during the GEMS and MACC projects. Details of the model can be found in Morcrette et al. (2009) and Benedetti et al. (2009) and we summarize here the main features.

Five types of tropospheric aerosols are considered: sea salt (SS), dust (DU), organic (OM) and black carbon (BC), and sulfate (SU) aerosols. Prognostic aerosols of natural origin, such as mineral dust and sea salt are described using three size bins each. Hygroscopic effects are considered for organic matter, black carbon, sulfates and sea salt which means a total of 11 prognostic variables. Emissions of dust depend on the 10-m wind, soil moisture, the UV-visible component of the surface albedo and the fraction of land covered by vegetation when the surface is snow-free with a correction to the 10-m wind to account for gustiness (Morcrette et al., 2008). Sea-salt emissions are diagnosed using a source function based on work by Guelle et al. (2001) and Schulz et al. (2004). Sources for the other aerosol types which are linked to emissions from domestic, industrial, power generation, transport and shipping activities, are taken from the SPEW (Speciated Particulate Emission Wizard), and EDGAR (Emission Database for Global Atmospheric Research) annual- or monthly-mean climatologies. More details on the sources of these aerosols are given in Dentener et al. (2006). Emissions of OM, BC and SO2 linked to fire emissions are obtained using the GFAS system based on MODIS satellite observations of fire radiative power, as described in Kaiser et al. (2011).

MODIS AOD data at 550 nm are routinely assimilated in a 4D-Var framework which has been extended to include aerosol total mixing ratio as extra control variable (Benedetti et al., 2009). A variational bias correction for MODIS AOD is implemented based on the operational set-up for assimilated radiances following the developments by Dee and Uppala (2008). The bias model for the MODIS data consists of a global constant that is adjusted variationally in the minimization based on the first-guess departures. Although simple, this bias correction works well in the sense that the CAMS analysis is not biased with respect to MODIS observations. The observation error covariance matrix is assumed to be diagonal, to simplify the problem. The errors are also chosen ad hoc and prescribed as fixed values over land and ocean for the assimilated observations. The aerosol background error covariance matrix used for aerosol analysis was derived using the Parrish and Derber method (also known as NMC method; Parrish and Derber (1992) as detailed by Benedetti and Fisher (2007). This method was long used for the definition of the background error statistics for the meteorological variables and is based on the assumption that

the forecast differences between the 48-h and the 24-h forecasts are a good statistical proxy to estimate the model background errors.

As explained in detail in Flemming et al. (2017), the total AOD in CAMSiRA shows a good agreement with surface-based AERONET observations, but problems have been identified with the way the data assimilation distributes the contribution of the various species to the total AOD, in particular introducing unrealistic high sulfates burden over the oceans. We therefore derived the climatological distribution of the 11 prognostic CAMS aerosol types using the Control Run (CR) set up alongside CAMSiRA and covering the period 2003-2014. This experiment uses the same meteorological fields and emission as CAMSiRA but without data assimilation, hence leaving the aerosol species free to evolve. We then used the total AOD from CAMSiRA to constrain this climatological AOD by scaling the monthly mean distribution of the individual species to reproduce the total AOD computed in the reanalysis. Therefore, each monthly-mean AOD for the single specie i at the grid-point (x,y) is adjusted following the simple relation:

$$AOD_{i,clim}(x,y) = \frac{AOD_{RA}(x,y)}{AOD_{CR}(x,y)} * AOD_{i,CR}(x,y) \tag{1}$$

where AOD_{RA} indicates the total AOD from the reanalysis, AOD_{CR} the total AOD from CR. Each specie is therefore scaled according to their contribution to the total AOD in a particular grid point.

The variable used in input to the radiation scheme has been modified from the total integrated AOD used in OPER climatology to the 3D mass mixing ratio for each aerosol components, consistent with the prognostic variables computed by the CAMS aerosol model. In order to reduce the size of the climatological files and the time spent in I/O, the aerosol distribution is read at run-time from a NetCDF file containing a monthly-mean spatial distribution of total column integrated mass $[kg/m^2]$ on a $3^\circ \times 3^\circ$ grid. This is then re-distributed vertically according to the analytical function discussed later in section 2.3. The monthly-mean distributions apply to the 15^{th} of each month and are linearly interpolated in time between the months as it was done for the OPER climatology.

2.1 Optical properties

The aerosol optical properties are computed for each of the 14 short-wave (SW) and 16 long-wave (LW) bands of the IFS radiation scheme (ECRAD, Hogan and Bozzo, 2016) assuming spherical particles for all species, with a number size distribution described by a log-normal function similar to the original version in Reddy et al. (2005) and defined as:

$$n(r) = \frac{dN(r)}{dr} = \frac{N}{\sqrt{2\pi}r\ln(\sigma)} exp\left(-\frac{\ln^2(r/r_{mod})}{2\ln^2(\sigma)}\right) \tag{2}$$

with N total particle number concentration, σ geometric standard deviation and r_{mod} mode radius. For the organic matter a mixture of optical properties provided in the OPAC database (Hess et al., 1998) are used.

Table 1 lists the relevant parameters of the distribution for each specie. The bulk optical properties (mass extinction coefficient, single scattering albedo (ω) and asymmetry parameter (g)) are computed with a standard code for Mie scattering (Toon and Ackerman, 1981). For the hydrophilic types the optical properties change with the relative humidity due to the swelling of the water soluble component in wetter

environments. The refractive index (m) and density (ρ) of the aerosol particle change according to the relations (Koepke et al., 1997):

$$\rho = \rho_{dry} * r_{dry}^3/r^3 + \rho_{water} * (r^3 - r_{dry}^3)/r^3 \quad (3a)$$

$$m = m_{water} + (m_{dry} - m_{water}) * r_{dry}^3/r^3 \quad (3b)$$

with r_{dry} and r the mode radius respectively of the dry particle and at a relative humidity value. The size distribution is modified applying growth factors (Table 2) to the mode radius and to the limits of integration, maintaining the same geometric standard deviation.

A brief description of the refractive index associated to each aerosol type is given in the following paragraphs.

Table 1: Refractive indices and parameters of the size distribution associated to each aerosol type in the CAMS model (r_{mod} =mode radius, ρ=particle density, σ=geometric standard deviation). Values are for the dry aerosol a part from sea salt which is given at 80%RH. The organic matter type is represented by a mixture of three OPAC types similar to the average continental mixture, as described in Hess et al. (1998). Three refractive indices are available for the dust type, see text for full details.

Aerosol type	size bin limits (sphere radius, μm)	Refr. index source	ρ (kg/m^3)	r_{mod} (μm)	σ
Sea Salt* (80% RH)	0.03-0.5 0.5-5.0 5.0-20	OPAC	1.183e3	0.1992,1.992	1.9,2.0
Dust	0.03-0.55 0.55-0.9 0.9-20	Dubovick et al. 2002/ Woodward et al. 2001/ Fouquart et al. 1987	2.61e3	0.29	2.0
Black carbon	0.005-0.5	OPAC (SOOT)	1.0e3	0.0118	2.0
Sulfates	0.005-20	Lacis et al. (GACP)	1.8e3	0.0212	2.24
Organic matter$^+$	OPAC-mixture	type	N (cm^{-3})	M ($\mu g/m^3$)	ρ (kg/m^3)
		WASO	12000	16.1	1.8e3
		INSO	0.1	2.4	2.0e3
		SOOT	8300	0.5	1.0e3

*Sea salt is described by a bi-modal log-normal distribution with fixed number concentrations of 70 cm^{-3} and 3 cm^{-3} for the small and the large mode respectively.

$^+$The hydrophobic component of organic matter uses the same optical properties but for a fixed relative humidity of 20%

Table 2: Growth factors used to characterize the size distributions of sea salt and sulfates

RH (%)	0	10	20	30	40	50	60	70	80	85	90	95
Sea salt	1.0	1.0	1.0	1.0	1.44	1.55	1.666	1.799	1.988	2.131	2.36	2.877
Sulfates	1.0	1.0	1.0	1.0	1.169	1.220	1.282	1.363	1.485	1.581	1.732	2.085

growth factors for sea salt are from Tang (1997), growth factors for sulfates are from Tang and Munkelwitz (1994).

Organic matter: The optical properties are based on the "continental" mixtures described in Hess et al. (1998). The mixture represents aerosols over continental areas influenced by anthropogenic and natural emissions. We used a combination of 13% in mass of insoluble soil and organic particles, 84% of water soluble particles originated from gas to particle conversion containing sulfates, nitrates and organic substances and a 3% of soot particles. The combination gives optical properties representing an average

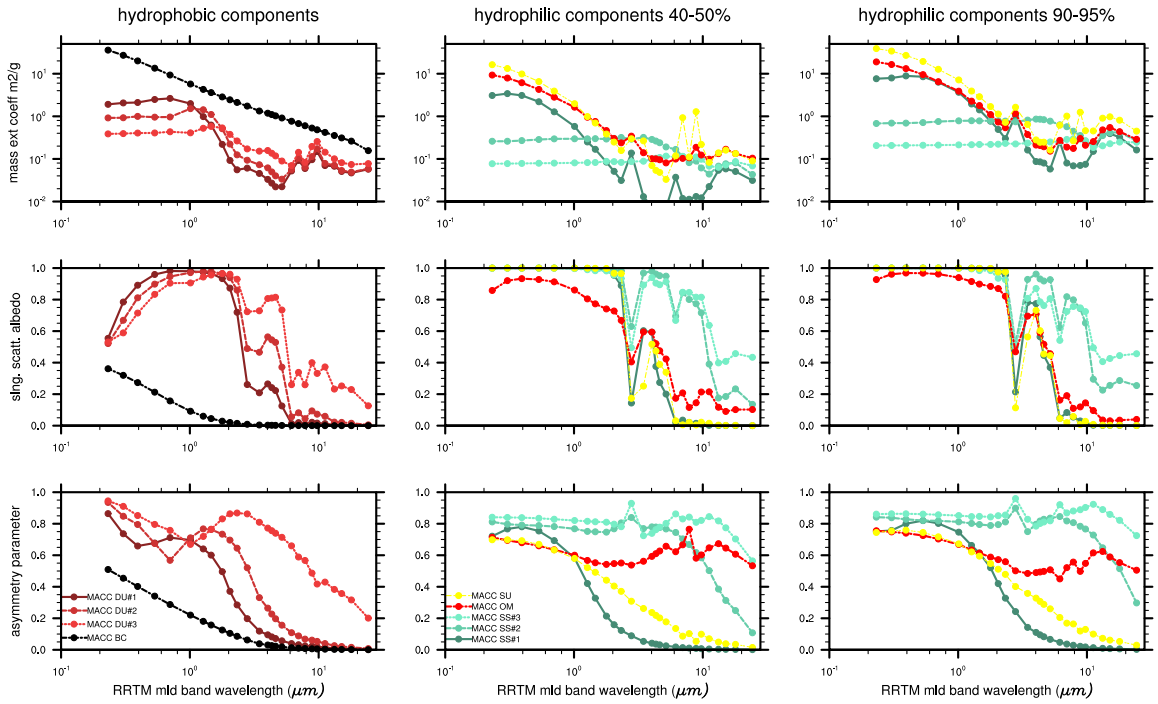

Figure 1: Optical properties of the aerosol species in the CAMS model for the 30 spectral bands of the ECMWF radiation scheme. For the hydrophilic species the mass extinction coefficient is computed with respect to the dry aerosol mass. The top row shows the mass extinction coefficient, the middle row shows the single scatter albedo and the bottom row shows the asymmetry parameter. The first column is for the hydrophobic species and the middle and right columns are for the hydrophilic species at two values of RH.

of biomass and anthropogenic organic carbon aerosols. The refractive indices and the parameters used in the particle size distribution of each component are as described in Hess et al. (1998). The hydrophobic organic matter type uses the same set of optical properties but for a fixed relative humidity of 20%.

Black carbon: The refractive index used in the Mie computations is based on the OPAC SOOT model. At the moment the hydrophilic type of the black carbon specie is not implemented and both types are treated as independent from the relative humidity. The single particle properties are integrated with a log-normal particle size distribution for sizes between 0.005 and 0.5 μm.

Sulfate: The sulfate type represents aerosol originated from sulfur emissions from industrial and fossil fuel combustion, biomass burning and natural sources (volcanic and biogenic). The refractive index is taken from the Global Aerosol Climatology Project (GACP, http://gacp.giss.nasa.gov/data_sets/) and it is representative of dry ammonium sulfate $(NH_4)2SO_4$. The hygroscopic growth is parameterized after Tang and Munkelwitz (1994) and reported in Table 2.

Mineral dust: The large uncertainty in mineral dust composition (e.g. Colarco et al., 2014) means that it is difficult to represent the radiative properties of this specie with a single refractive index fitting different part of the World. Three choices are at the moment available in the IFS, differing mainly in the SW dust absorption properties. Woodward (2001) combined measurements from different locations and provides the largest absorption in the visible range with an imaginary refractive index at 500 nm of $n_{i,500} = 0.0057$. Fouquart et al. (1987) propose a much smaller value $n_{i,500} = 0.0013$ and it represents the lower bound for mineral dust absorption. Dubovik et al. (2002) used AERONET measurements to retrieve the refractive index of mineral dust in different locations. For the Sahara region they report $n_{i,500} \sim 0.0022$ representing

a value in between the previous two. The optical properties are computed individually for each of the three size intervals in the CAMS mineral dust model, using a log-normal size distribution with limits 0.03, 0.55, 0.9, 20 μm. The impact of using different refractive index for mineral dust will be explored in section 4.1.

Sea salt: The refractive index for sea water is as in the OPAC database and the optical properties are integrated across the three size ranges in the CAMS model, using bi-modal lognormal distributions with limits 0.03, 0.05, 5, 20 μm as in Reddy et al. (2005) and with the same hygroscopic factors according to Tang (1997), Table 2.

The complete set of bulk optical properties for all aerosol types, is shown in Figure 1 for the full range of spectral bands used in ECRAD. Hydrophilic types in wetter conditions show larger total extinction and reduced absorption (larger ω). Large differences are evident in the three size bins of sea salt and mineral dust with the small size bin providing stronger extinction and less absorption than the larger size bin in the SW, while the opposite is observed in the LW.

This set of optical properties shows large differences when compared to the set used in the OPER climatology and this explains many of the changes in the aerosol radiative effect between the two climatologies discussed in the following sections. Particularly large are changes in the radiative properties of mineral dust and sulfates (Figure 2). The properties used to represent the desert dust in the OPER climatology produce large absorption in the SW range 0.4-2 μm with $\omega = 0.75$ at 550 nm while the new properties, when using the Woodward (2001) refractive index, have smaller absorption with ω at 550 nm ranging from 0.97 to 0.85, respectively for the smallest and the largest of the size bins. The relatively weak absorption of mineral dust in the short-wave is supported by an increasing body of research (e.g. Kim et al., 2011; Balkanski et al., 2007; Haywood et al., 2003; Dubovik et al., 2002) which indicates that earlier estimates of ω for dust might have been biased too low.

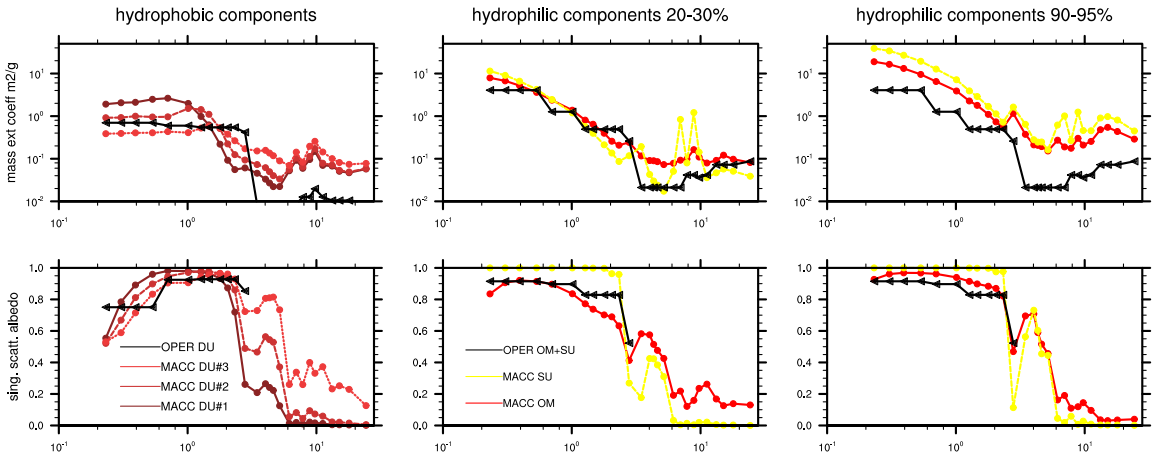

Figure 2: Comparison between the bulk optical properties of mineral dust (left) and sulfates and organic matter (centre and right for two values of RH) as used in the OPER climatology and in the CAMS climatology. Data for the 30 spectral bands of the ECMWF radiation scheme. For the hydrophilic species the mass extinction coefficient is computed with respect to the dry aerosol mass. Top row shows the mass extinction coefficient and bottom row the single scatter albedo.

As for sulfates and organic matter, these were previously represented together, implying a low ω for the sulfates type in the SW range (0.91 at 550 nm). Sulfates are now treated independently from the organic specie with virtually no absorption in the SW.

2.2 Spatial distribution

The distribution of the AOD at 550 nm for each individual type and for their sum shows marked regional and seasonal variations (Fig. 3). The largest contributions to the total AOD comes from the mineral dust and the organic matter associated to the emissions from various anthropogenic and natural processes. The sea salt is the main contributor to the total AOD in the southern Ocean and in the Northern Hemispere storm tracks. The sulfates are generally well distributed but the largest AOD is found close to the sources of anthropogenic emissions.

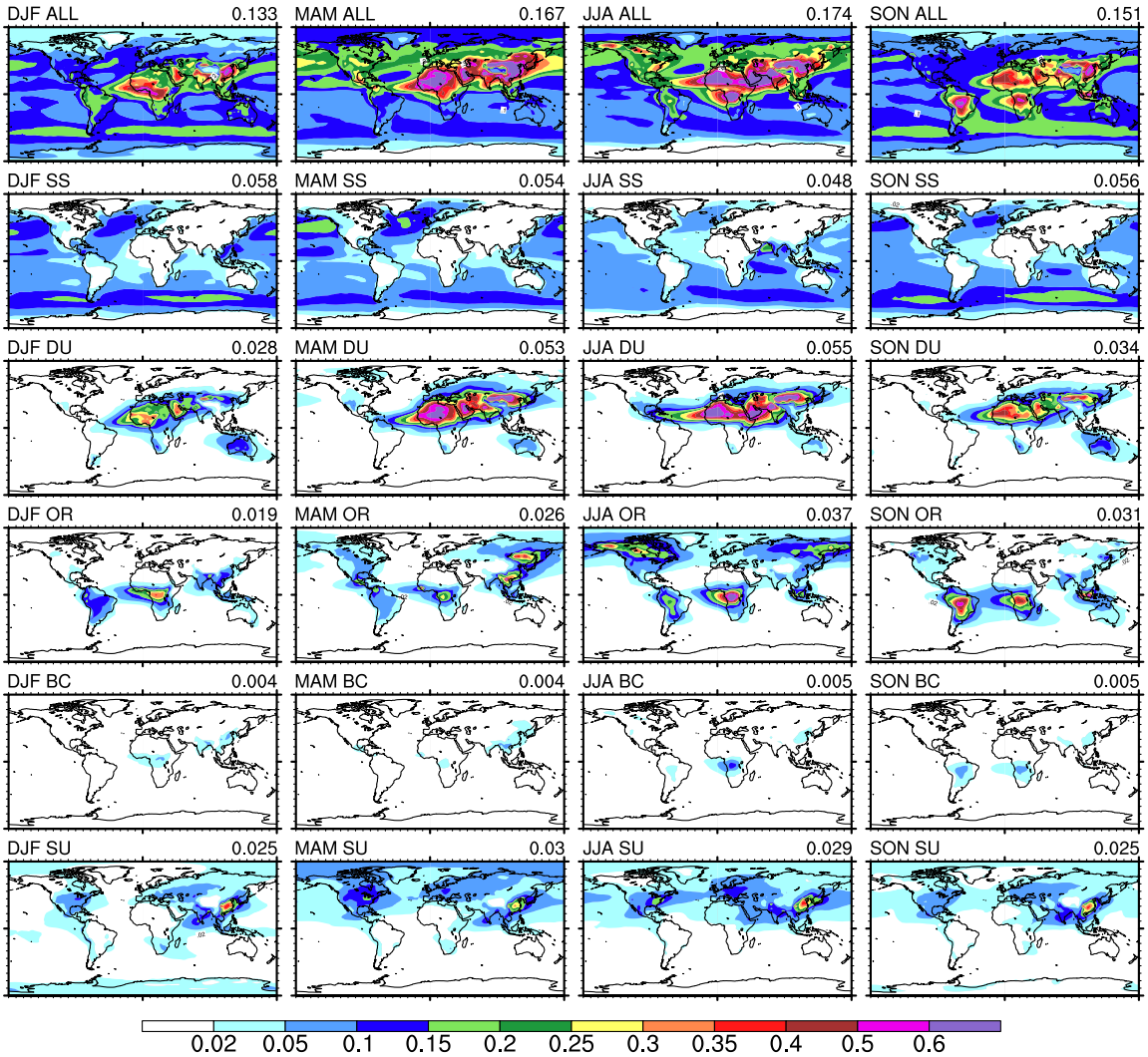

Figure 3: Seasonal aerosol optical depth at 550nm from the CAMS Interim reanalysis control run, scaled to conserve the total AOD of the assimilation run. The top row shows the total optical depth and the other rows the contribution from the single species for each season. Indicated in the top right of each map is the global average.

Very large are the differences with respect to the aerosol distribution from the OPER climatology, as observed already in Morcrette et al. (2011) (Fig. 4a). In the CAMS climatology the total AOD from the sea salt is much larger and it dominates the differences in the Southern Hemisphere.The mineral dust has a much larger AOD over the deserts and a significantly different spatial distribution, with the JJA maxima reduced over the Horn of Africa, Australia and South America and increased over the Sahara and Middle East. The organic matter and black carbon have significantly larger burden in the regions characterized by strong biomass burning as over central Africa, the western Amazon forest, the south-eastern Asia and northern Canada. Finally, in the CAMS climatology there is less transport of organic and sulfate aerosol over the Equatorial Eastern Pacific, particularly for the DJF trimester.

Given the change in the optical properties associated to each specie, the absorption AOD shows even larger differences between the two climatologies (Fig. 4b). Although the total AOD in the dust regions is larger in the CAMS climatology than in the OPER climatology, this contributes to a smaller fraction of the total SW absorption because of the change in the dust optical properties. Over Europe, Asia and Central-North America it is the small amount of anthropogenic aerosols in the CAMS climatology that is responsible for the reduction in absorption in those regions. This presumably highlights the difference in the emissions between the periods used to build the two climatologies. Anthropogenic emissions over industrialised regions of Europe and North America have shown as being in decline since the '90s with detectable impact on surface radiation fluxes (Wild, 2009, 2012) while the opposite has been observed for the Eastern Asia and India. The differences in absorption AOD between the two climatologies could also suggest a too low emission of absorbing aerosols of anthropogenic origin in the CAMS system (Flemming et al., 2017).

Since the introduction of the OPER climatology a well mixed background aerosol is added on top of the monthly varying climatology both in the troposphere and in the stratosphere, with a total AOD in the 0.4-0.6 microns band of 0.05 and 0.045 respectively. The tropospheric background shares the optical properties of the organic matter type while in the stratosphere the background represents the average amount of pure sulfate aerosols left after large volcanic eruptions.

Being an homogeneously distributed absorbing specie, the tropospheric background has non-negligible impact on the model mean climate and on the mean forecast errors, acting essentially as a tuning parameter for the radiative fluxes. Ideally the CAMS climatology would not need an extra background AOD in the troposphere but we noticed a non negligible impact on the IFS forecast skill scores and more careful investigation is required to understand whether this is due to compensating errors affecting the mean tropospheric temperature. For the present implementation of the CAMS climatology, we left the background level to the same total AOD of 0.05 in the band 0.4-0.6 microns, but using the new optical properties of the organic matter type, at a fixed relative humidity of 20% as done for the hydrophobic specie. This means that the effective background extinction AOD in the range 0.2-1.5 microns is slightly higher with slightly lower ω than before (see Fig 2). The effect of including a background AOD in the IFS is discussed in detail in section 4.2.

Recent estimates of the variability in the stratospheric background aerosol concentration in quiet times between large volcanic eruptions, show values of total AOD at 500 nm between 0.004 and 0.005 (Solomon et al., 2011; Bourassa et al., 2012) which is 10 times smaller than the value currently assumed in the OPER climatology (Fig. 5). For the CAMS climatology the stratospheric background AOD has been set to 0.0045. The impact of this change is small and it amounts to a global increase of about 1 W/m^2 in the clear-sky SW radiation reaching the mid troposphere.

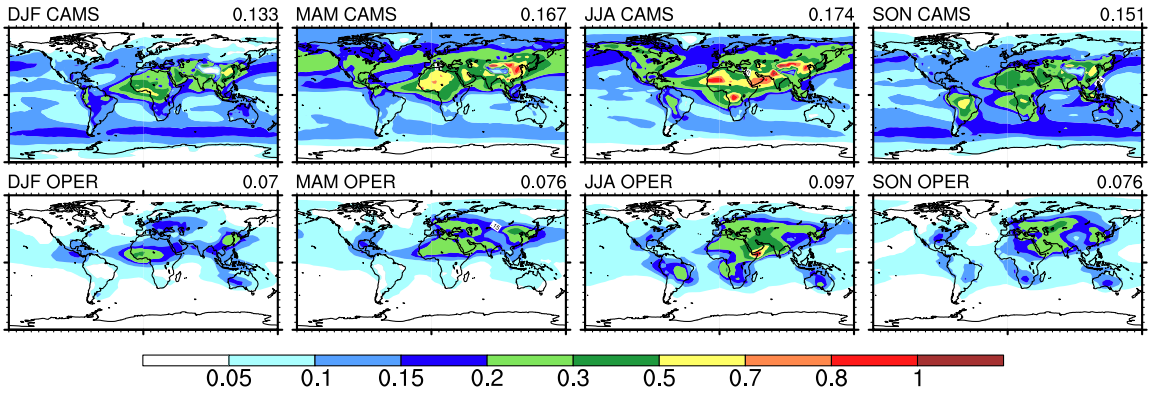

[a]

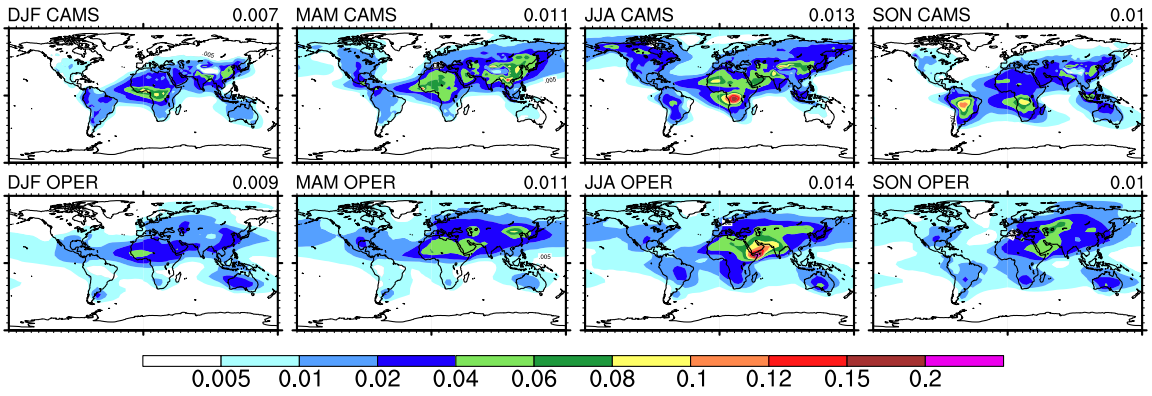

[b]

Figure 4: Seasonal total extinction (a) and absorption (b) aerosol optical depth at 550nm. CAMS interim reanalysis control run, scaled to conserve the assimilated AOD (top row) and the current operational climatology (bottom row). The single scattering albedo used to compute the absorption for the hydrophilic species is representative of an average relative humidity of 50%-60%. Notice the different scale for the two panels.

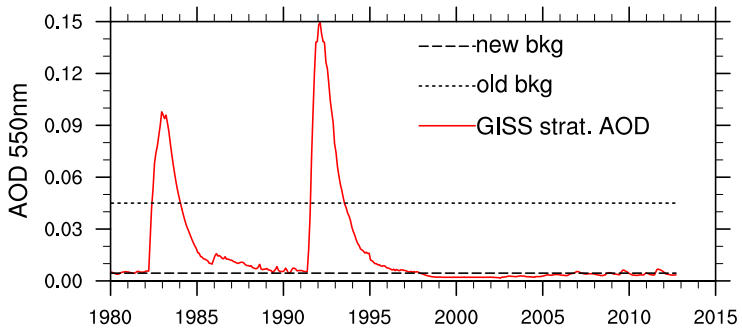

Figure 5: Time series of total stratospheric aerosol optical depth at 550 nm from 1980 to 2012. The two black lines show the values of the constant background value used in the OPER and in the CAMS climatology. The estimate of the stratospheric AOD time series comes from the forcing used in the GISS climate simulations (https://data.giss.nasa.gov/modelforce/strataer//)

2.3 Vertical distribution

The aerosol distributions are specified in the IFS as 2-D fields of integrated total column mass. In the implementation of the CAMS climatology we adopted the same vertical distribution of the aerosol species used in the OPER climatology, but modified to better reflect the 3D structure of the aerosol fields in the CAMS model. Using 2D fields the total size of the climatology input files is reduced to ∼8 Mb from the ∼450 Mb of the 3D fields (when using a spatial grid of 3°x3° and 60 vertical levels) speeding up the run time reading and interpolation process.

The aerosol cumulative vertical mass distribution is computed starting from the total integrated column mass, using a pressure-dependent function of the form $(p/p_0)^{(H/\xi)}$, with p_0 pressure at the lowest model level, $H = 8.4$ km the scale height of the standard atmosphere and ξ the scale height of the aerosol component. The mass mixing ratio on the model vertical levels is then computed from the vertical cumulative mass profile.

We used the CAMSiRA-scaled AOD from CR to estimate the scale height ξ for each aerosol type, which depends on the aerosol spatial distribution and the season. This is found by calculating at every grid point the height at which the normalized cumulative mass distribution reaches the value $1/e$. The spatial distribution of ξ is shown in Fig 6 for July and January for all aerosol types.

Mineral dust and sea salt show a dependence on the size bin, but this is small with a slightly lower ξ for the coarser sizes. There is a large spatial variations in ξ between the source regions, where the aerosol distribution tends to be closer to the surface, and the regions of advection, where the mass is lifted to higher levels according to the seasonal atmospheric patterns. This broad picture is consistent with combined estimates using CALIPSO lidar observation, MODIS AOD retrievals and prognostic aerosol models (Yu et al., 2010; Winker et al., 2013).

We approximated ξ with a single global-mean value for each of the five main types, averaging the values estimated from the CR at each grid point. We limited the impact of regions with very low aerosol concentrations by weighting the local ξ by the total AOD of that aerosol type. For dust and sea salt the AOD is the total across the three size bins.

The ξ of mineral dust exhibits the largest spatial and seasonal variations because of the strong depen-

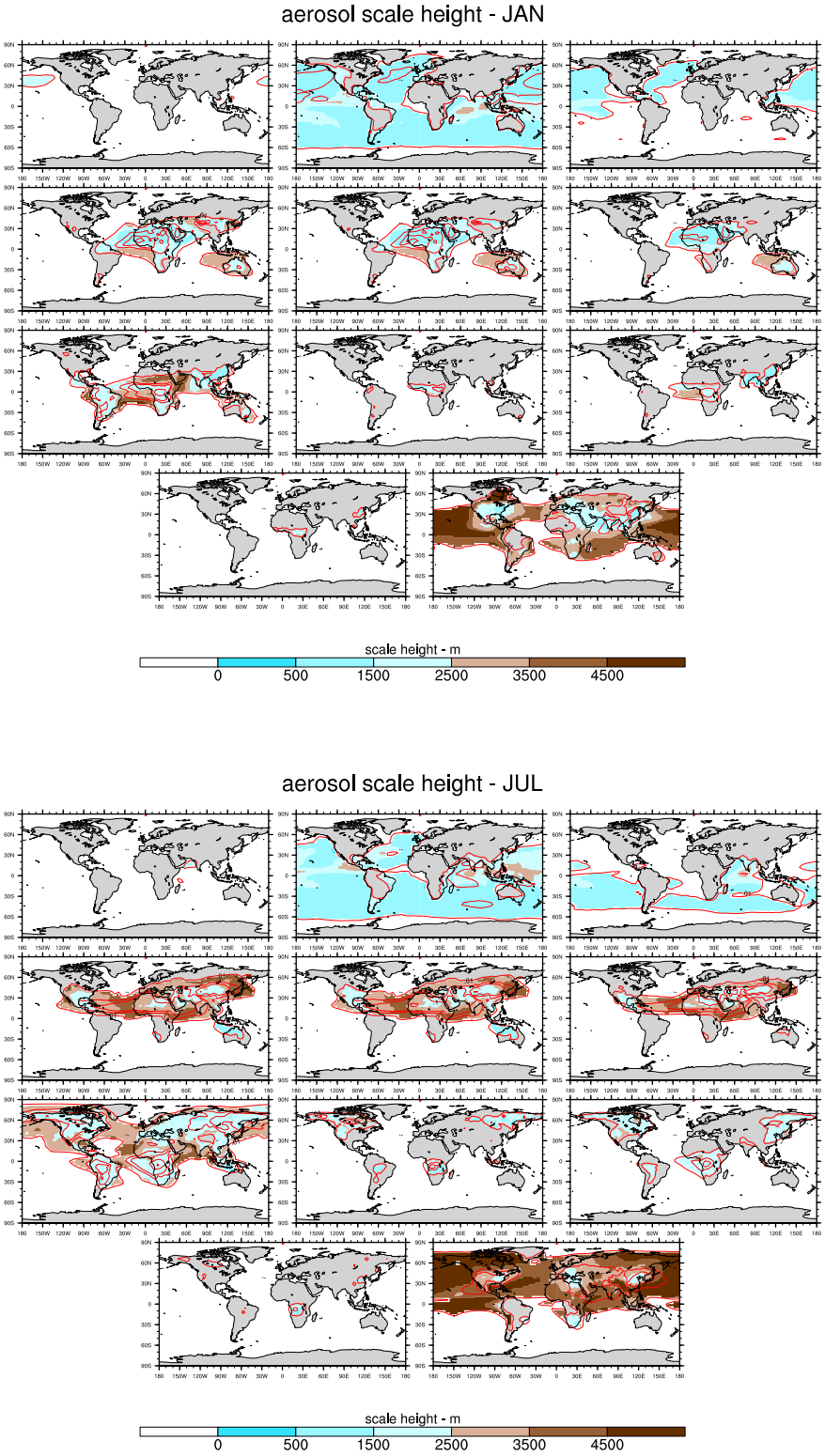

Figure 6: Scale height (color shade) and AOD (red contours) for each aerosol type computed from the CAMS free-running forecasts over the years 2003-2011 and with the total AOD scaled to preserve the CAMS reanalysis total AOD. The scale height is shown only for the grid points with an AOD for that aerosol type larger than 0.01. Aerosol types are, starting from top left: SS1,SS2,SS3,DD1,DD2,DD3,OR1,OR2,BC1,BC2,SU. Contour lines values are 0.01,0.05,0.1,0.4,0.8,1

dence of the dust sources on the height of the boundary layer mixing over the deserts and the seasonal patterns of large-scale advections. Given the large seasonal cycle, the mineral dust type is the only specie employing a monthly varying ξ ranging from 2 km in winter rising to 3 km in summer. For the other species we used a constant value throughout the year. Sea salt aerosols and black carbon are generally confined to the lower levels with $\xi \sim 1$ km, while the organic matter extends higher with $\xi \sim 2$ km. As sulfate is formed from SO_2 it occurs further away from the sources and tends to have a more homogeneous distribution with $\xi \sim 3$ km (Fig 6).

The analytical vertical mass distribution reproduces reasonably well the climatological zonal-mean distribution of the different species (Fig 7), but there are obviously evident limits in a simple pressure-dependent distribution with a single global-mean scale height. This is more evident in the Northern-Hemisphere summer months when the local maximum in the AOD profile observed in CR tends to be spread over more layers by the analytical representation. The vertical distribution of mineral dust exhibits a large spatial variability and this limits the possibility to use a single global-mean parameter to represent it. Over the biomass burning area of Central Africa the elevated maximum of the organic and black carbon species are squeezed to lower levels. This could potentially have implication in the total radiative effect of these species which is affected by their relative vertical position with respect to cloud layers. Compared to a reference experiment with a constant $\xi = 1$ km for all species, we found that only for mineral dust the details of the vertical distribution have a significant impact on the model climate and forecast skill because this specie has relatively large AOD over wide areas (not shown).

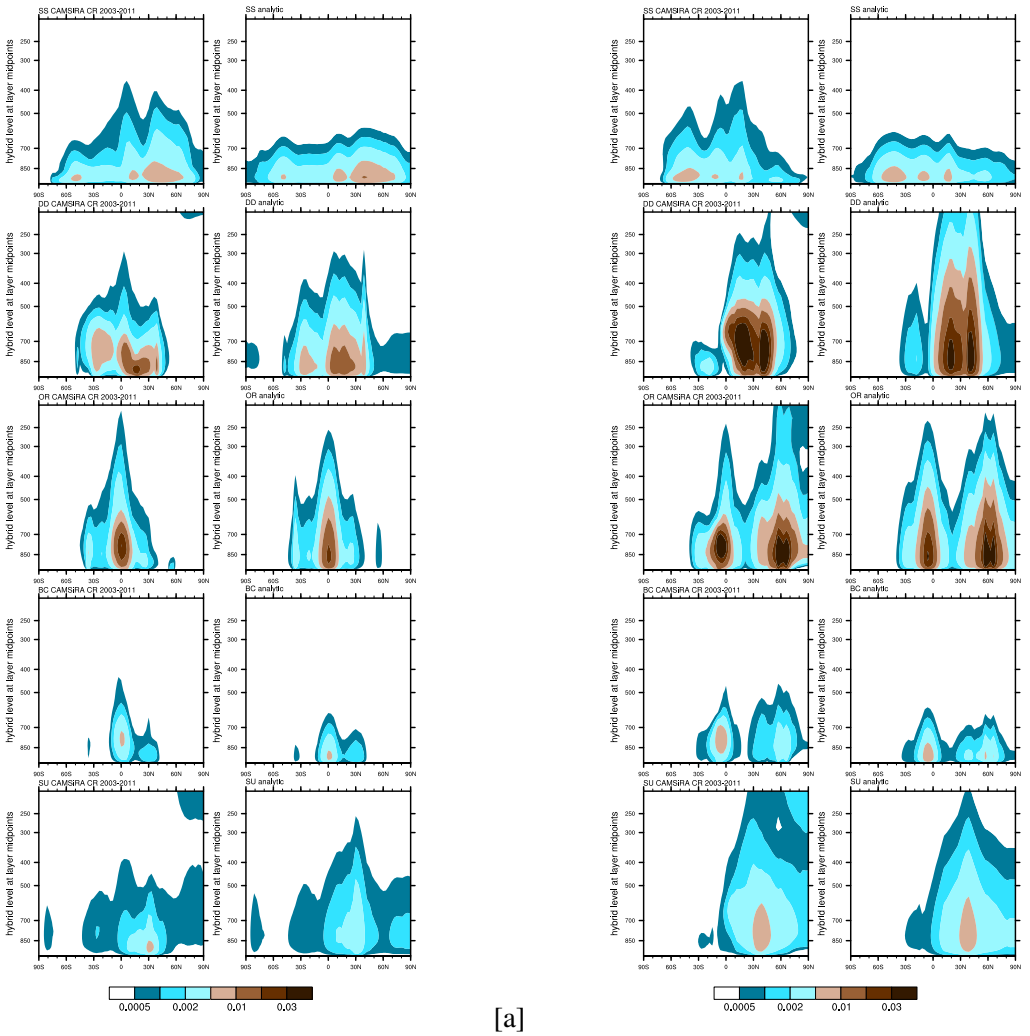

Figure 7: Zonal-mean extinction optical depth profiles, weighted by the total integrated optical depth at every grid point. Monthly average for January (panel a) and July (panel b). Left column: the vertical profile for the CAMS CR scaled to preserve the CAMSiRA total AOD. Right column: vertical profile for the climatology using the scale height estimated from the control run.

3 Impact on radiative fluxes, heating rates and model climate

The change from the OPER to the CAMS climatology directly impacts radiative fluxes and heating rates both in the LW and SW. At the surface the CAMS climatology induces a reduction in net clear-sky SW flux of about 2.7 W/m^2 but values reach 20-30 W/m^2 in the larger AOD in the biomass burning areas and over the deserts (Fig 8b-e). The larger amount of sea-salt aerosols over the oceans also contributes to a reduction of the surface net clear-sky SW radiation by about 2-4 W/m^2. Both in the winter and in the summer months the AOD in the CAMS climatology is smaller over Europe causing an increase in the surface SW radiation by about 5 W/m^2.

At the TOA the CAMS climatology increases the clear-sky reflected SW radiation globally inducing a reduction of net SW flux between 1.5 and 2.0 W/m^2. On one hand this is related to the larger amount of sea salt aerosols and to the larger dust plumes advected from the Sahara desert over the Atlantic Ocean and on the other hand it is the result of higher reflection from regions dominated by the dust

specie (Fig 8a-d). A larger total AOD over Antarctica together with the slightly larger tropospheric aerosol background level adopted in the CAMS climatology causes a reduced SW reflection south of 70 S during the Austral summer increasing the net SW flux (Fig 8a). This effect is likely to be overestimated because of a too large aerosol load over the Antarctic Continent in the CAMS model.

The impact on the LW fluxes is small but significant in the regions with the largest mineral dust AOD in the Northern Hemisphere summer months (Fig 8g-h). At the surface there is an increase of downwelling LW radiation reaching more than $10 W/m^2$ over the Western Sahara and Saudi Arabia, in part compensating the reduction of net SW radiation there. At the TOA significant differences are found only where the high-level dust layers reduce the up-ward emission to space over the desert areas.

The increased reflectivity of the mineral dust aerosols means less net SW absorption over the desert in areas where the two climatologies have comparable AOD. This is the case over Saudi Arabia and the Middle-East in summer where there is a reduction of SW absorption of about 4-8 W/m^2 and up to 30 W/m^2 over the Horn of Africa (Fig. 8f). Over the Western Sahara and in the biomass burning regions the AOD is larger than in the OPER climatology and this increases the SW absorption significantly. Globally the new climatology increases the mean atmospheric SW absorption by 0.5 to 1.0 W/m^2.

Changes in TOA total-sky radiative fluxes are smaller than for clear sky, but there are local improvements to model biases when compared to CERES-EBAF top of atmosphere observations. For an ensemble of four one-year integration experiments with prescribed SST (Fig 9) biases in the SW flux are improved over the Western Sahara and the Central-East Atlantic as well as part of the Middle-East and Indian Ocean. Improvements in roughly the same areas are also visible for the LW fluxes, in particular the reduction in out-going LW radiation (OLR) over Western Sahara and the increase in OLR over the Indian Ocean. These changes are a combination of direct radiative impact of the modified aerosol layer for predominantly clear sky areas such as the Western Sahara region and indirect feedbacks on regional circulation modifying the cloud cover for areas like the Indian Ocean.

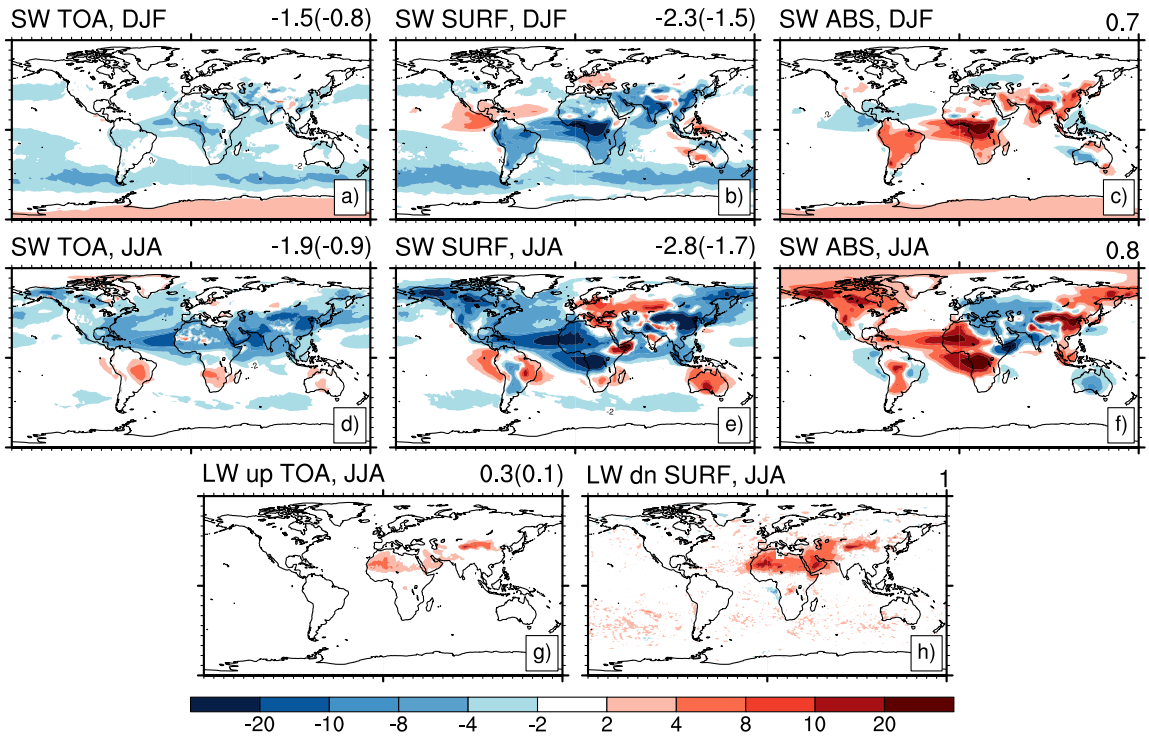

Figure 8: Changes radiative fluxes between the new CAMS climatology and the OPER climatology. Panels a to f: changes in the clear-sky net short-wave radiation at the TOA(a,d), surface(b,e) and net short-wave atmospheric absorption (c,f) for January and July. Panels g,h: changes clear sky in TOA up-welling (g) and all-sky surface down-welling (h) long-wave radiation. Net fluxes are defined as down-welling minus up-welling. Values are given in W/m^2. In the top right corner of each sub plot is indicated the global mean for clear sky (all-sky). Fluxes are the average over the five days from the 15^{th} to the 19^{th} of June,July and August(December, January and February) for the summer(winter) forecast experiments.

4 Impact on forecast errors and skill

Changes in the aerosol radiative effect impact mostly the model mean state and affect to a small extent measures of large-scale forecast skill scores. Although the change in AOD is highly inhomogeneous and locally large, this does not appear to be enough to impact the variability of the large-scale circulation. The direct impact of new aerosol climatology is to perturb the radiative heating rate profiles and the surface energy budget. The former dominates the change in forecasts errors, and it affects the mid-to-lower tropospheric temperatures. The latter has some impact on the surface temperature.

Large areas dominated by mineral dust experience a reduction in absorption of SW radiation and this induces a widespread decrease in temperature of about 0.1 K below 700 hPa after 48h (Fig 10) growing to more than 0.2 K at day five. This reduces by about a third the positive temperature bias observed in the operational model in the Mediterranean region and the Middle-East. The effect is larger in the summer months due to the stronger mean insolation and the larger dust AOD.

Another significant temperature change is observed below 850 hPa over the Gulf of Guinea and Central Africa where the relatively large amount of biomass burning aerosol in the CAMS climatology absorbs a

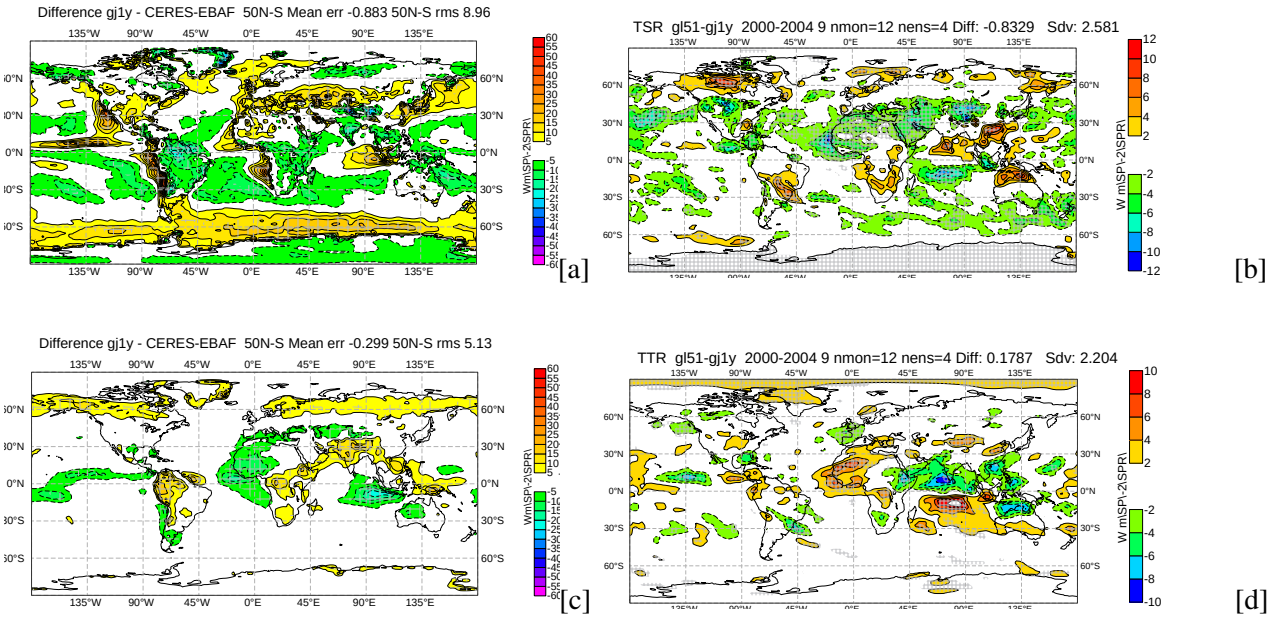

Figure 9: Changes in multi-annual mean (2001-2004) top of atmosphere error in short-wave (top row) and long-wave (bottom row) fluxes. Operational IFS against CERES-EBAF observations (a,c). Changes in the top of atmosphere fluxes for an experiment with the CAMS climatology compared to the operational IFS (b,d). Hatching represents differences at a significance level of 5%.

significant amount of SW radiation increasing the positive bias of the region. The biomass burning specie have generally a small but positive impact on the upper-air temperature biases over Northern Canada in the summer months.

The impact on surface temperature is very localized and significant only over Central and North Africa and part of Asia (Fig 11), where changes in the AOD between the two climatologies is the largest (see Fig 4). In the biomass burning regions of Central Africa the decrease in surface SW radiation causes a decrease in the surface temperature which opposes a pre-existent positive bias. In North Africa and Middle-East the impact of change in dust cover is significant in the summer months, with surface cooling over the West Sahara dominated by the reduction in down-welling SW and surface warming over Saudi Arabia where the significant increase in down-welling LW compensate the smaller decrease in down-welling SW. Other significant temperature changes are found in Australia, where the reduction in dust AOD in the CAMS climatology causes surface warming and in the Taklamakan desert where the large dust AOD causes surface cooling.

The effect of the new CAMS climatology on the variability and forecast skill of large-scale extra-tropical weather patterns is negligible with not significant changes in the anomaly correlation of mid-tropospheric geopotential (not shown), similar to results of Morcrette et al. (2011). Measurable changes are found for the temperature RMSE in the lower troposphere (fig 12), due to changes in both the standard deviation and the mean bias of forecasts errors discussed above. In particular, for the tropical temperature at 850 hPa RMSE decreases by $\sim 1\% - 0.5\%$ in the winter months while it increases by the same amount in the summer months. The degradation in summer is mostly dominated by the localized increase in forecast errors over the Gulf of Guinea (local increase in the RMSE up to 20%) which affects the mean error standard deviation over the tropics. Given the scarce availability of surface observations it is difficult to have a good estimate of the correct aerosol radiative effect in the area but perhaps these errors could indicate

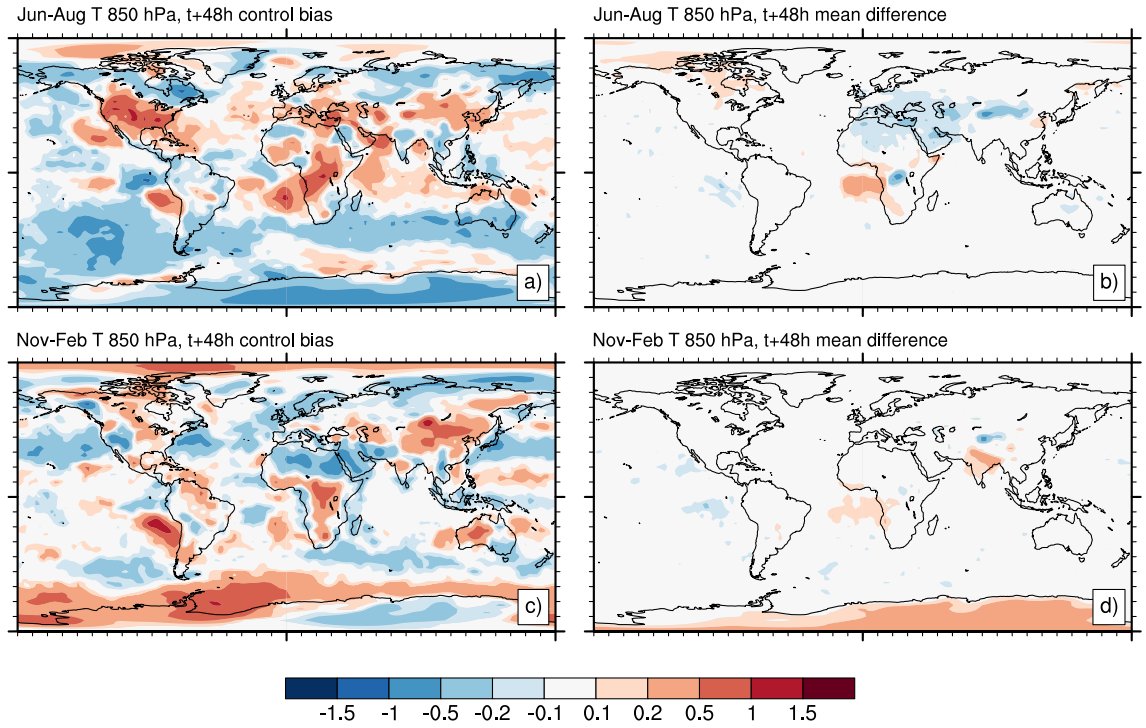

Figure 10: Difference in temperature at 850 hPa (K) for forecast time t+48 hours between operational forecasts and own analysis (a,c) and between a forecast experiment with CAMS climatology and the operational model (b,d).

a possible bias in the CAMS aerosols in the region. Estimates of absorption AOD in the area (e.g. Bond et al., 2013) seem indeed to suggest a large overestimation in the CAMS model in the summer months over Central Africa, although at the moment it is not clear whether this is related to the distribution of biomass burning or rather to the assumption in the composition and ageing properties of the main species responsible for non optimal optical properties.

The temperature RMSE generally improves in the Northern Hemisphere by about 1% in summer thanks to the reduction in the mean bias over the dust regions between the surface and 700 hPa.

Although the changes brought about by the CAMS aerosol climatology do not affect significantly the large scale circulation, impacts at regional scale are stronger. The largest changes are located over the Indian Ocean during the summer Monsoon season and are forced predominantly by a modified radiative forcing by the desert dust which brings a reduction in the near-surface wind errors. Section 5 presents in more details the feedbacks between the Monsoon circulation and changes the local AOD.

4.1 Uncertainty in dust radiative properties

As discussed in Section 2.1, uncertainty in the chemical composition of mineral dust reflects in uncertainty in its radiative properties which in turn affects the impact that the dust AOD has on model forecast errors. Further uncertainty can also be expected from assumptions in the particle size distribution and

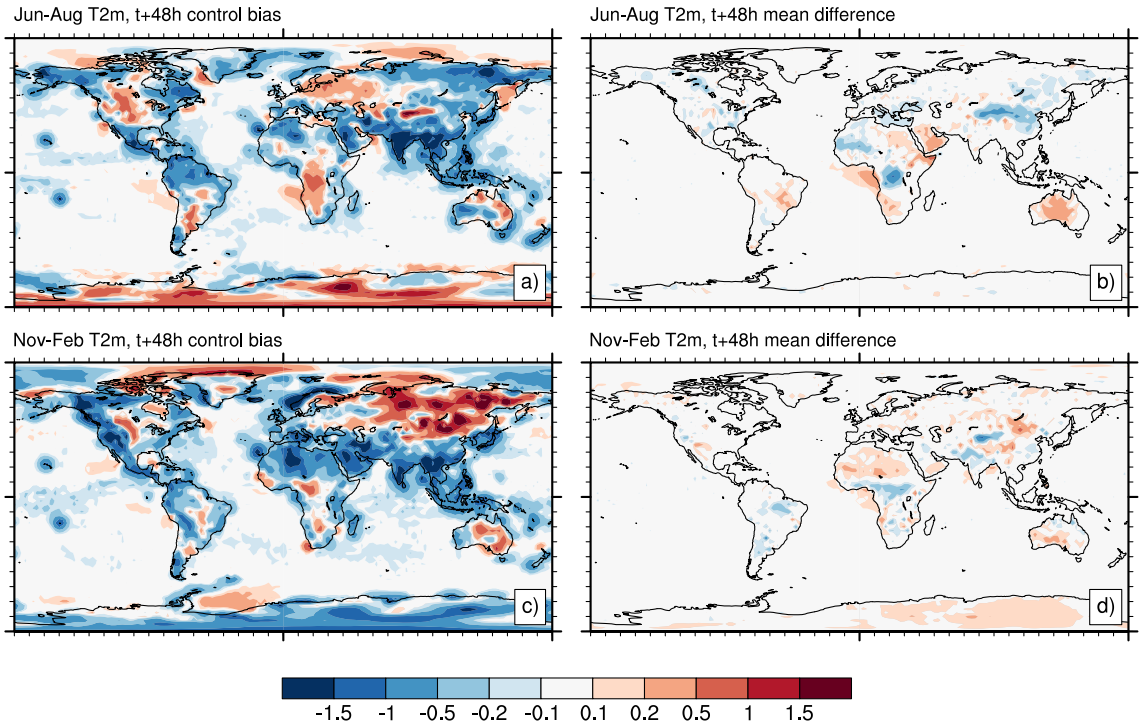

Figure 11: As Fig 10 but for 2 m temperature.

particle shape used to describe the dust aerosol in the CAMS system (e.g. Colarco et al., 2014), but a detailed investigation of these aspects is beyond the scope of this technical report.

We compared in two separated forecast experiments the impact of using optical properties computed with the dust refractive indices suggested by Woodward (2001) and by Dubovik et al. (2002). The major difference is significantly more absorption in the SW range for the set based on Woodward (2001) (Table 3).

Table 3: Dust optical properties for the ECRAD band 400-700 nm computed using different refractive indices (mass extinction coefficient $k, m^2/g$, single scattering albedo ω and asymmetry parameter g). Data are for each of the three size bins of the CAMS aerosol model (limits 0.03, 0.55, 0.9, 20 μm)

RI	k	ω	g
Woodward (2001)	2.5,0.95,0.4	0.96,0.90,0.83	0.68,0.67,0.80
Dubovik et al. (2002)	2.4,0.98,0.4	0.98,0.96,0.92	0.65,0.67,0.76

The direct impact of the two set of radiative properties for dust is on the mean tropospheric temperature over the desert regions, which is lower in the experiment with the weakly absorbing dust (Fig 13). As already shown in Fig 10, in the summer months a certain degree of cooling in the lower troposphere in the dust regions has a positive impact on the temperature biases in the Northern Hemisphere and this effect is enhanced using Dubovik et al. (2002) refractive index. But pre-existing cold biases are also enhanced, especially in the Northern Hemisphere in the winter months and in the Tropics, and this has an overall detrimental impact on the temperature over large areas as seen looking at the changes in the

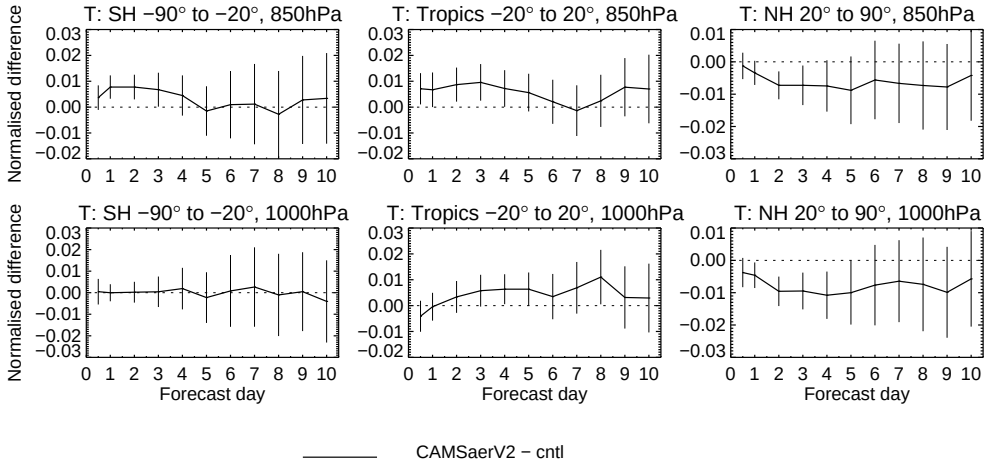

[a]

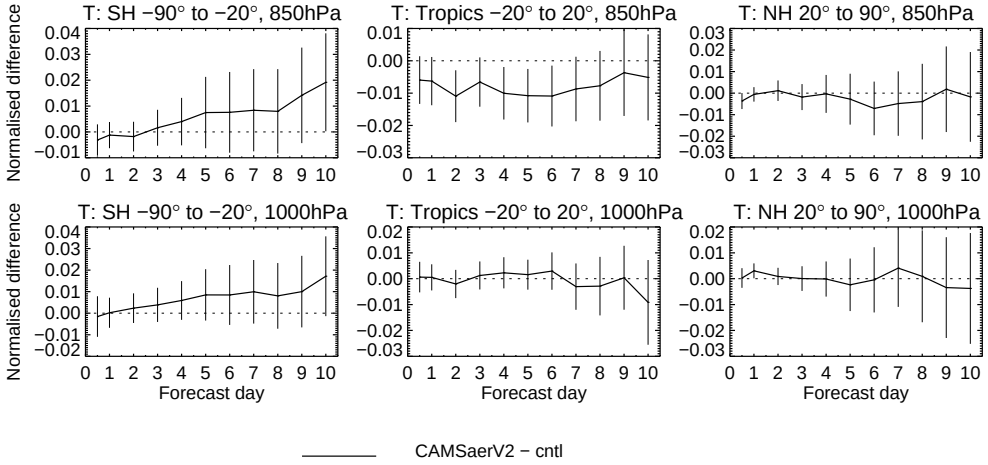

[b]

Figure 12: Normalized temperature RMSE difference at 1000 hPa and 850 hPa for a set of forecasts using the new CAMS climatology against the operational configuration. The experiments cover a summer season (2-May-2016 to 13-Aug-2016, [a]) and winter season (2-Nov-2015 to 28-Jan-2016, [b]) and are verified against own analysis. Confidence range 95% with AR(2) inflation and Sidak correction for 4 independent tests. These experiments have an horizontal resolution of Tco399 but the main results are independent on the model resolution.

temperature RMSE in Fig 13.

The sensitivity of the large scale skill scores to the choice of the dust refractive index is small with a slight degradation in the temperature RMSE in the NH winter and with negligible impact on the variability of the large-scale hemispheric circulation (not shown). But areas which are particularly sensitive to dust radiative forcing show higher sensitivity, with surface winds over the northern Indian Ocean and in Western Africa responding to the enhanced cooling forced by the more reflective dust (Fig 14).

The mineral dust aerosols are the dominant specie over large areas and therefore uncertainty in their radiative forcing has the potential to affect model biases as shown by these experiments. The current choice of the Woodward (2001) dust refractive index together with the particle size distribution described in Section 2.1 gives the least 'aggressive' change to model skill scores still providing a general improvement of mean model biases, yet it is likely that it still overestimates the SW absorption by dust in the near visible

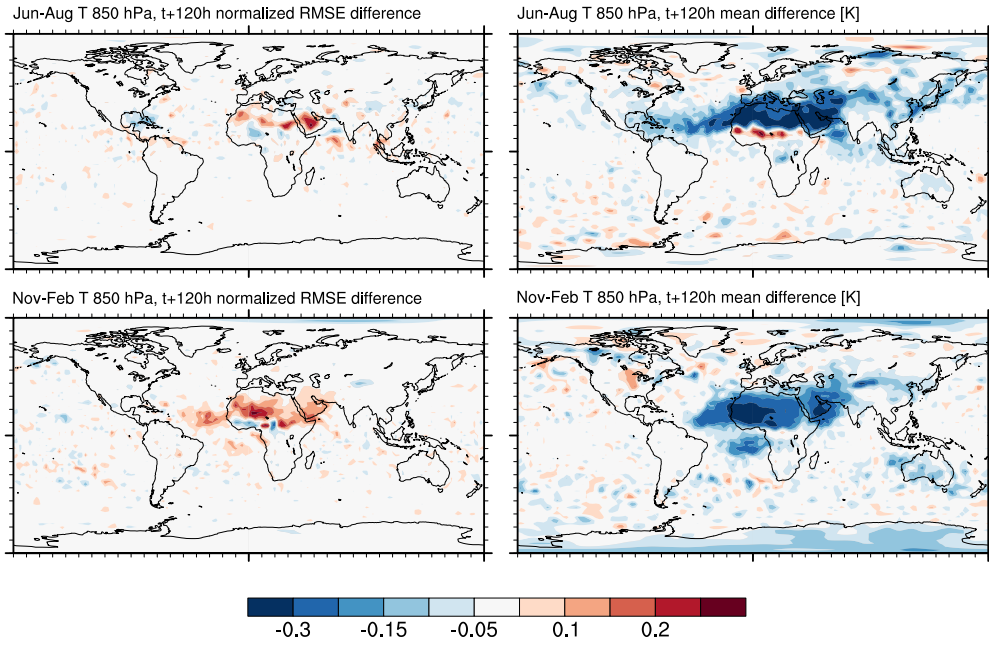

Figure 13: Mean difference and normalized difference in RMSE for temperature at 850 hPa at forecast day 5 between the experiment using the mineral dust refractive index from Dubovik et al. (2002) and from Woodward (2001). Average over a series of forecasts for summer (Jun-Aug 2015) and winter (Nov-Feb 2015-2016). Reference to compute the RMSE is the operational analysis.

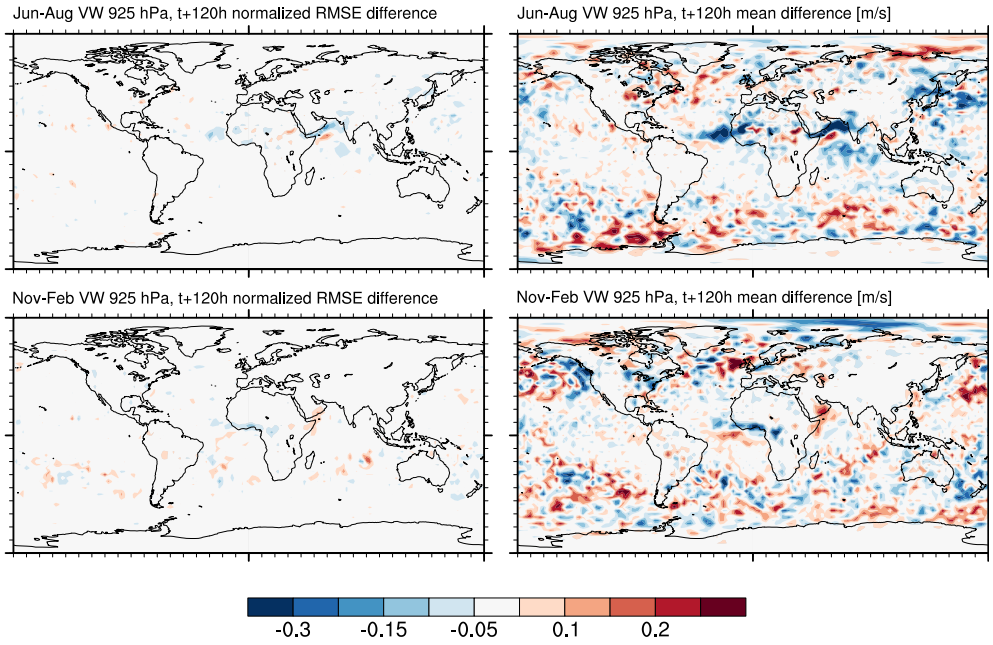

Figure 14: As Fig 13 but for the vector wind at 925 hPa.

wavelengths (Kim et al., 2011; Balkanski et al., 2007; Haywood et al., 2003). More work is needed to better understand the link between model biases and these uncertainties and exploit their potential to improve the model mean climate and local circulations.

4.2 The need for a background aerosol in the troposphere in the IFS and its impact on the forecast skill scores

As mentioned in section 2.2, a well mixed tropospheric background aerosol is added to the current OPER climatology. This aerosol type is described by the same radiative properties used by the organic specie, with a total optical thickness of 0.05 in the SW band 0.4-0.7 μm and a constant vertical rate of change of optical thickness with pressure of 0.037/atm up to the tropopause. This background was originally introduced with the earlier annual mean climatology based on Tanré et al. (1984) and it was maintained when the current Tegen et al. (1997) climatology was introduced. Its impact on the radiative fluxes is not negligible especially in the SW.

The radiative effect of the background aerosol is to increase the clear-sky reflected SW flux at TOA by about 1.0 W/m^2 and by about 1.3 W/m^2 the total SW absorption by the atmosphere. This together brings a reduction in the incoming clear-sky SW flux at the surface by about 2.3 W/m^2. When removed, the mean temperature in the troposphere decreases by about 0.05 K after 5 days and up to 0.1 after 8 days in the upper levels (Fig. 15). This affects the hemispheric model skill scores particularly in the tropics and above 500 hPa (Fig. 16) with a significant degradation in the RMSE due to the fact that in the upper troposphere the model already develops a cold bias with lead time.

Although in principle the new CAMS climatology should provide a complete representation of the aerosol load in the atmosphere, the uncertainty in the assimilated MODIS AOD (Levy et al., 2010) leaves some room for adjustment in the representation of a mean climatological total AOD. But the effect that this parameter has on the model mean state and the interaction with pre-existing model errors makes it difficult to handle. The need for an aerosol background could also indicate a compensation for the lack of radiative heating from some radiative source currently not adequately represented.

For the time being we maintained the tropospheric background because of its significant impact on the model skill scores. But further work is needed to better understand why the model benefits from this extra tuning parameter and possibly remove the need for it.

5 Impacts on local circulations: the summer Indian Monsoon

The area of the Northern Indian Ocean during the summer Monsoon season shows the largest feedback between changes in aerosol radiative forcing and regional-scale circulation. In this region the CAMS climatology has a different impact on radiative fluxes than the OPER climatology (Fig 4 and Fig 8). The largest change during summer is a decrease in total SW absorption over the Middle-East and East Africa of approximately 4-8 W/m^2 on average, but exceeding 30 W/m^2 over the Horn of Africa. This is due to both a change in the distribution of mineral dust mass in the region and to the higher dust reflectivity in the CAMS climatology (Fig 2). Total (SW+LW) surface fluxes show generally an increase in down-welling radiation bringing a small increase in surface temperature (Fig 11).

Numerous studies have explored the sensitivity of the summer Indian Monsoon to aerosol radiative forcing from both anthropogenic and natural sources (Bollasina et al., 2011; Lau and Kim, 2006; Wang et al., 2009). By using a combination of model and satellite data Vinoj et al. (2014) showed that the radiative

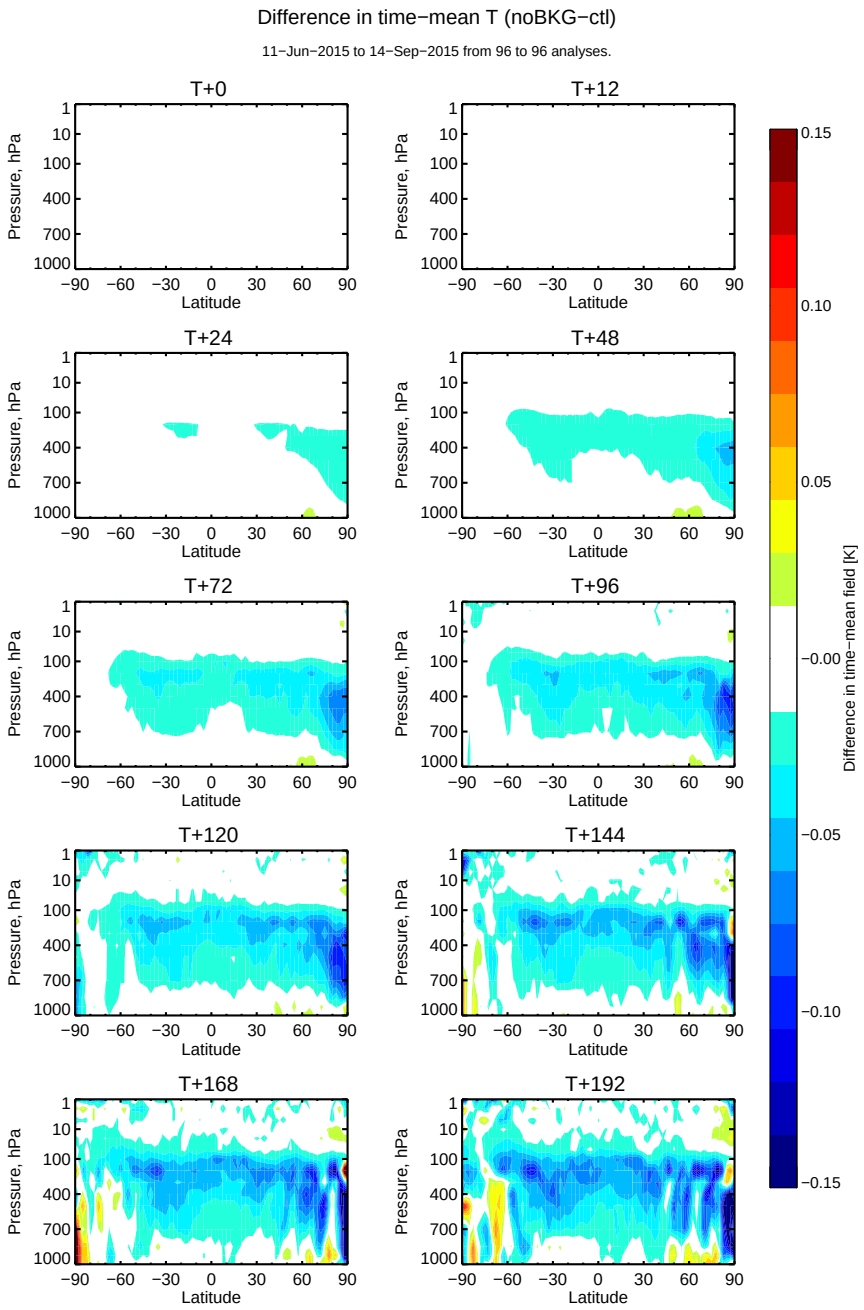

Figure 15: Difference zonal mean temperature as function of forecast lead time between a set of forecasts without and with a tropospheric aerosol background of 0.05 total optical thickness in the 0.4-0.7 µm band. Both experiments use the OPER climatology and cover the period 11th June 2015 to 14th September 2015.

effect of mineral dust over Eastern Africa and Arabian Peninsula affects the Monsoon circulation over the Indian Ocean. The heating rate perturbation induced by the dust layer can modulate the strength of low level westerly zonal winds and moisture transport towards Eastern and Central India over time scales of weeks. This implies that a realistic representation of the aerosol radiative effect in the region can potentially have a significant impact on the predictability of the Monsoon circulation in medium-range and seasonal forecasts.

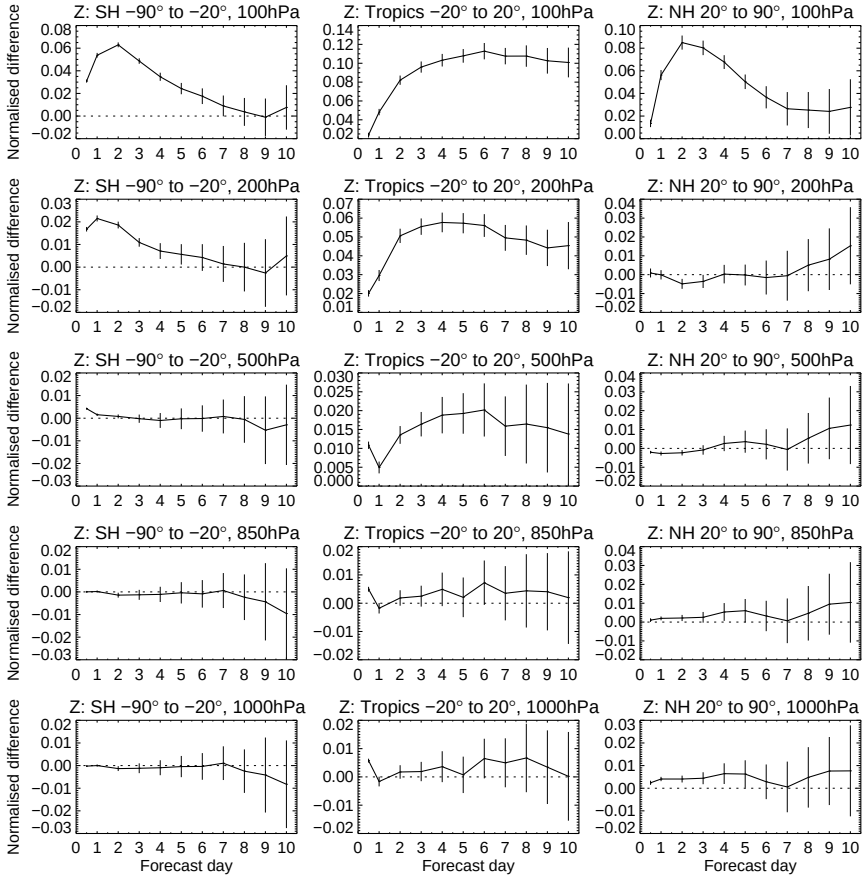

Figure 16: Normalized difference in geopotential height RMSE between a set of forecasts without and with a tropospheric aerosol background of 0.05 total optical thickness in the 0.4-0.7 µm band. Both experiments use the OPER climatology and are verified against the operational analysis over the period 11th June 2015 to 14th September 2015. The vertical bars show the 95% confidence level with an inflation factor based on AR(1) noise and the Sidak correction for 4 independent tests. Values above zero indicate that the forecast performance degrades when the background aerosol is removed.

In the operational configuration with prescribed sea-surface temperatures the IFS has a too strong near-surface westerly jet across the northern Indian ocean, from the Eastern Africa to the Western India (Fig 17a) which in turns causes too wet conditions over Western India during the summer months. This brings a positive precipitation bias in the region of 1-2 mm/day over the three month period June-August as compared to various estimates of surface precipitation (Table 4). The same circulation bias is also responsible for the positive error of the top-of-atmosphere outgoing long-wave radiation (see Fig 9c), related to too much cloudiness over Western India.

The CAMS climatology forces changes in the mean winds and temperature mostly below 700 hPa and this reduces the forecasts errors in the area both for the wind strength at all lead times (Fig 17b) and also for the cumulated seasonal errors in precipitation amounts (Table 4). The increase in surface temperature and pressure over the Persian Gulf and Saudi Arabia reduces the first-guess departures (Fig. 18) indicating an improvement in the analysis fields.

Near-surface zonal wind strength decreases in the northern part of the Indian Ocean and increases to the south (Fig 17b), implying a weakening and southward shift of the low-level jet. Indeed also the

Table 4: Mean precipitation over Western India (region boundaries: lat 25N-6N;lon 67E-77E) for JJA estimated by different products and model bias for two forecast experiments for the period 2001 to 2004. Data are in mm/day.

	GPCP v2.2	HOAPS3 v6*	SSMI*	TRMM nasda 3b43
OBS	5.5	5.1	2.5	6.4
OPER-OBS	2.1	0.2	4.1	1.3
CAMS-OBS	1.4	-0.3	3.8	0.5

*values not defined on land grid points

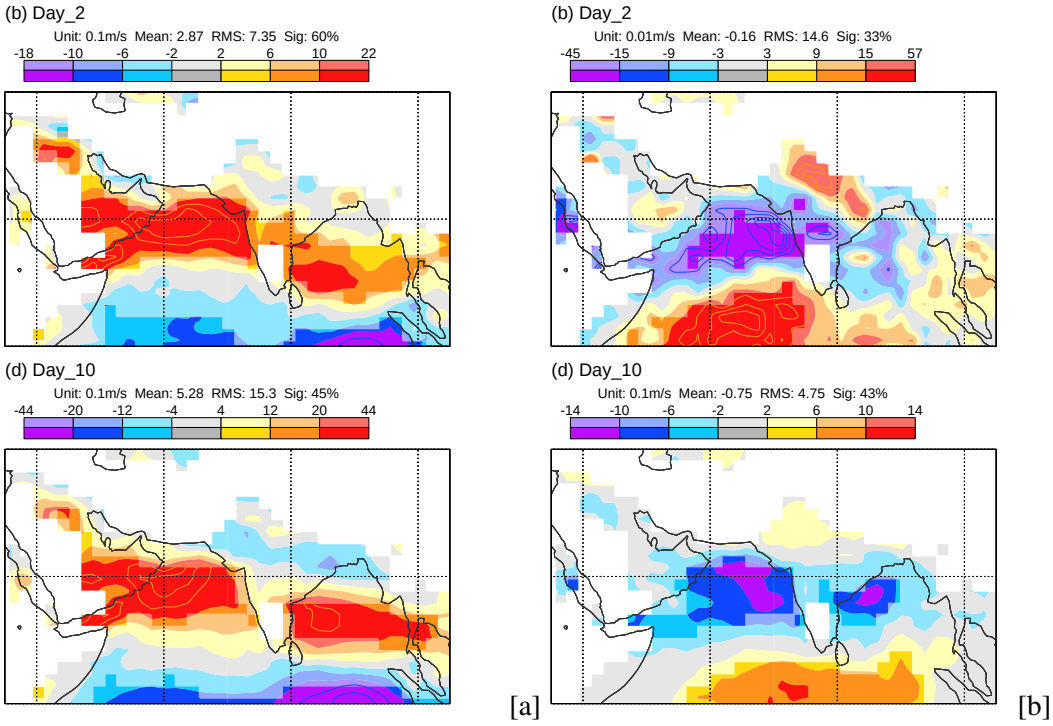

Figure 17: Near surface (925 hPa) zonal wind for the period 1st of May 21st of August 2016 over the northern Indian Ocean for forecast day 2 (top) and 10 (bottom). Operational model bias (a) and difference between forecasts using the CAMS climatology and the OPER climatology (b). Notice the different scales between the right- and the left-hand side panels. Bold colors indicate areas significant at the 5% level using a paired T-test with AR(1) noise.

change in the meridional wind component shows a weakened northward flow close to the Horn of Africa between the surface and 850 hPa (not shown) confirming an overall reduced north-eastward circulation. The changes grow larger at longer lead times due to the cumulative contribution of the modified radiative forcing acting from the very beginning of the forecast.

These circulation changes are the result of a combination of large-scale and more localized perturbations to the temperature gradients between the Indian Ocean and the land areas.

In the CAMS climatology less SW radiation is absorbed by the dust layer causing a decrease in the lower tropospheric temperature over the Eastern Africa/Arabic peninsula region (see Fig. 10), a key driver of the Monsoon circulation in the Indian Ocean (Vinoj et al., 2014). Following this lower tropospheric cooling, the geopotential height decreases over land above 500 hPa inducing upper level convergence and localized descending motion which partially balances the radiative cooling. This causes an increase in the surface pressure and geopotential height at low levels over the Middle-East and Arabian peninsula,

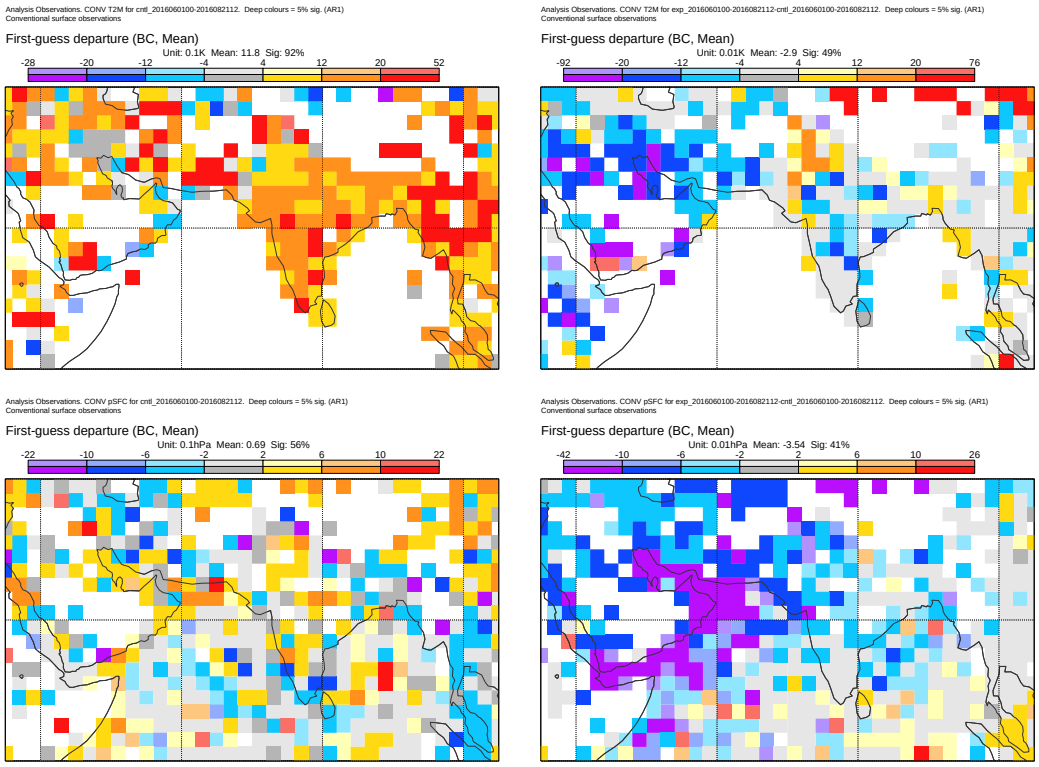

Figure 18: First guess departures (observations-model) for 2m temperature and surface pressure for the period 1st of Jun to 21st of August 2016 against conventional surface observations. Operational departures (left column) and difference in departures between an experiment using the CAMS climatology and the operational configuration (right column). Bold colors indicate areas significant at the 5% level using a paired T-test with AR(1) noise. Negative values on the right hand side indicate that the experiment is closer to the observations than the operational configuration.

improving the model bias by up to 30%-50% in the lowest levels (Fig 19). The higher pressure below 800 hPa reduces the low-level convergent flow over the continental areas resulting in a weaker north-eastward circulation in the northern section of the Indian Ocean.

Running the same simulation with the less absorbing dust optical properties from the Dubovik et al. (2002) refractive index, we obtain stronger lower tropospheric cooling in the region and as consequence also a stronger response by the atmosphere (Fig 14). This sensitivity, together with the fact that in our experiments the SST are prescribed and that we do not explicitly simulate the interaction between aerosol and cloud microphysics, proves that the direct atmospheric heating by the dust layer is the main factor behind the observed circulation changes.

As a further step to investigate the impact of aerosol radiative forcing in the area it would be interesting to run a similar experiment using the full prognostic CAMS scheme. Given the interaction with the local circulation and the fact that dust sources depend on the wind strength, it should be possible to observe feedbacks on the dust production which could impact the representation and predictability skill of the Monsoon circulation over the Indian Ocean and western India. On a smaller scale, similar feedbacks have been reported in case of large dust storm outbreak over Sahara where changes in the surface radiative balance affected surface winds and in turn mineral dust production (Rémy et al., 2015). On a larger scale, Colarco et al. (2014) reported changes in the dust lifetime when including prognostic dust radiative effects in the NASA GEOS-5 model.

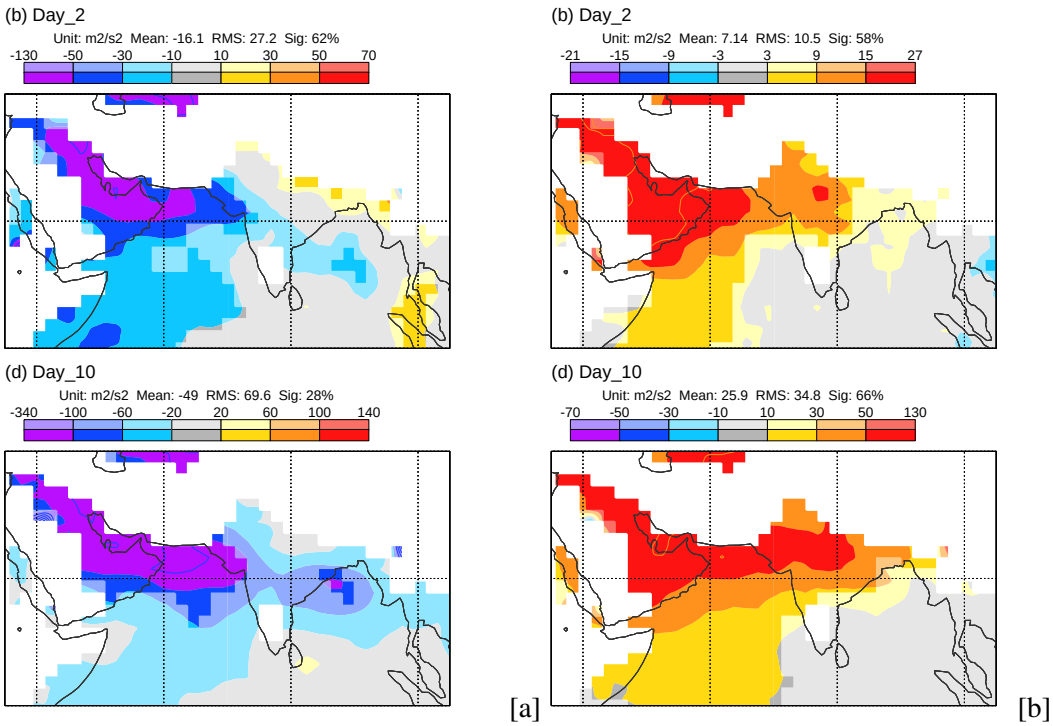

Figure 19: Geopotential height at 925 hPa for the period 1st of May 21st of August 2016 over the northern Indian Ocean for forecast day 2 (top) and 10 (bottom). Operational model bias (a) and difference between forecasts using the CAMS climatology and the OPER climatology (b). Bold colors indicate areas significant at the 5% level using a paired T-test with AR(1) noise.

6 Summary and future work

This technical report documents the implementation in the operational IFS of a new monthly-mean climatology of aerosol distribution based on the latest version of the atmospheric composition modules coupled to the IFS (C-IFS) used in the CAMS interim Reanalysis (CAMSiRA, Flemming et al., 2017). This new climatology substitutes the current aerosol climatology based on Tegen et al. (1997) introduced in 2003. The aerosol radiative properties have been computed individually for each of the 11 types of the CAMS aerosol model and the influence of the ambient humidity is taken into account for the hydrophilic species. The 3D distribution of each aerosol type is computed analytically from the 2D monthly-mean column-integrated mass at each grid point to reduce the size of the input files.

The new CAMS aerosol climatology modifies the radiative fluxes and improves locally biases both in the short-wave and in the long-wave spectrum compared to satellite observations. The change in aerosol radiative forcing with respect to the old climatology is due to both a different spatial distribution of the aerosol species and to the update of their radiative properties. The most significant contribution to the total aerosol radiative forcing comes from the mineral dust, organic and black carbon species.

The impact of the modified aerosol radiative forcing is largest for the mean lower-tropospheric temperature with a decrease in short-wave absorption and cooling over areas dominated by dust AOD and stronger absorption with warming in areas with large amount of organic matter and black carbon from natural and anthropogenic sources.

The summer Indian Monsoon over the Indian Ocean shows a marked sensitivity to the mineral dust ra-

diative forcing over Eastern Africa and Saudi Arabia. The more reflective mineral dust in the CAMS climatology modifies the temperature gradients over the Indian Ocean affecting the north-eastward branch of the the Indian Monsoon. The modified circulation improves by about 30% the model errors in temperature, zonal wind and precipitation over the northern Indian Ocean and Western India.

The new aerosol climatology has a nearly neutral impact on hemispheric forecast skill scores and virtually no impact on the variability of the large-scale synoptic circulation, in agreement with recent results of Morcrette et al. (2011); Mulcahy et al. (2014); Toll et al. (2016). The lower tropospheric temperature RMSE shows some sensitivity to the change in the aerosol short-wave radiative forcing, especially during the Northern Hemispheric summer. Improvements are observed over the Middle-East and the Mediterranean while an increase in bias dominates the Central Atlantic close to the central African coast due to overestimated absorption from species related to seasonal biomass-burning sources.

This implementation of the CAMS aerosol climatology is the first revision in the treatment of the aerosols in the operational IFS since the introduction of the Tegen et al. (1997) climatology and it opens the possibility to further improvements also taking advantage of the on-going development of C-IFS in CAMS. In particular there are few areas that could potentially affect the IFS and will need attention in the next version of the climatology.

- Since the first introduction of an aerosol climatology in IFS, a well-mixed tropospheric background aerosol was added to tune the total AOD. The radiative impact of this background aerosol is significant and it overlaps with pre-existent model biases, making it difficult to modify. With the introduction of the new CAMS climatology we should no longer need this extra specie but more work is required to carefully asses its impact on the model biases.

- The vertical distribution of the aerosol types in the CAMS climatology is improved with respect to the previous climatology but it is still not optimal. Future work should test the sensitivity of the model to a full 3D climatological aerosol distribution both in terms of forecast skills and computational burden.

- We have shown that mineral dust is one of the species with the largest impact on model biases and potentially on regional forecast skill. The uncertainty in its optical properties should be exploited to improve its radiative effect in the most sensitive areas such as Western Africa and the Middle-East. Further work should also explore at which spatio-temporal scales the model could benefit from having this type as prognostic variable.

- Large errors were found in the Gulf of Guinea linked to aerosols produced by biomass burning sources developing seasonally over land in Central Africa. This calls for an increased attention in the evaluation of the quality of C-IFS aerosol fields not only in terms of total extinction AOD but also in terms of absorption AOD (AAOD). This is a difficult task though given the difficulty in the estimate of AAOD and the sparse observation network.

The present CAMS climatology is based on an interim reanalysis which is part of the preparatory work towards the next complete CAMS reanalysis of atmospheric composition. Therefore, once the new reanalysis will be available, a further revision of this climatology will also be available and it will include the further improvements made to C-IFS since CAMSiRA was produced.

Acknowledgements

We thank Irina Sandu, Robin Hogan and Richard Forbes for their valuable comments at various stages of this work. Also a thank to the CAMS consortium for their work towards the improvement of the atmospheric composition modules coupled to the IFS and for their efforts in the evaluation of the atmospheric composition products.

References

Balkanski, Y., Schulz, M., Claquin, T., and Guibert, S., 2007, Reevaluation of Mineral aerosol radiative forcings suggests a better agreement with satellite and AERONET data, *Atmos. Chem. Phys.*, 7, 81-95, doi:10.5194/acp-7-81-2007.

Benedetti, A., J.-J. Morcrette, O. Boucher, A. Dethof, R. J. Engelen, M. Fisher, H. Flentje, N. Huneeus, L. Jones, J. W. Kaiser, et al., 2009: Aerosol analysis and forecast in the European Centre for Medium-Range Weather Forecasts Integrated Forecast System. Part 2: Data assimilation, *J. Geophys. Res.-Atmospheres*, 114(D13), D13205, doi:10.1020/2008JD011115.

Benedetti, A., and M. Fisher, 2007: Background error statistics for aerosols, *Q. J. R. Meteorol. Soc.*, 133, 391 405.

Bellouin, N., Boucher, O., Haywood, J., and Reddy, M. S.: Global estimate of aerosol direct radiative forcing from satellite mea-surements, *Nature*, 438, 11381141, 2005.

Bellouin, N., J. Rae, A. Jones, C. Johnson, J. Haywood, and O. Boucher (2011), Aerosol forcing in the Climate Model Intercomparison Project (CMIP5) simulations by HadGEM2-ES and the role of ammonium nitrate, *J. Geophys. Res.*, 116, D20206, doi:10.1029/2011JD016074.

Bollasina, M., Ming, Y. and Ramaswamy, V. Anthropogenic aerosols and the weakening of the South Asian summer monsoon. *Science* 334, 502-505 (2011).

Bond, T. C., et al., 2013, Bounding the role of black carbon in the climate system: A scientific assessment, *J. Geophys. Res. Atmos.*, 118, 53805552, doi:10.1002/jgrd.50171.

Boucher, O., D. Randall, P. Artaxo, C. Bretherton, G. Feingold, P. Forster, V.-M. Kerminen, Y. Kondo, H. Liao, U. Lohmann, P. Rasch, S.K. Satheesh, S. Sherwood, B. Stevens and X.Y. Zhang, 2013: Clouds and Aerosols. In: Climate Change 2013: The Physical Science Basis. Contribution of Working Group I to the Fifth Assessment Report of the Intergovernmental Panel on Climate Change [Stocker, T.F., D. Qin, G.-K. Plattner, M. Tignor, S.K. Allen, J. Boschung, A. Nauels, Y. Xia, V. Bex and P.M. Midgley (eds.)]. Cambridge University Press, Cambridge, United Kingdom and New York, NY, USA, pp. 571658, doi:10.1017/CBO9781107415324.016.

Boucher, O., M. Pham, and C. Venkataraman, 2002, Simulation of the atmospheric sulfur cycle in the Laboratoire de Meteorologie Dynamique general circulation model: Model description, model evaluation, and global and European budgets, *Note Sci. IPSL 23, 27 pp., Inst. Pierre Simon Laplace, Paris*. (Available at http://www.ipsl.jussieu.fr/poles/Modelisation/NotesSciences.htm)

Bourassa, A.E., A. Robock, et al., 2012, Large volcanic aerosol load in the stratosphere linked to Asian monsoon transport. *Science* 337, 78-81, doi:10.1126/science.1219371.

Colarco, P. R., E. P. Nowottnick, C. A. Randles, B. Yi, P. Yang, K.-M. Kim, J. A. Smith, and C. G. Bardeen, 2014, Impact of radiatively interactive dust aerosols in the NASA GEOS-5 climate model: Sensitivity to dust particle shape and refractive index, J. Geophys. Res. Atmos., 119, 753-786, doi:10.1002/2013JD020046.

Dee, D. and S. Uppala, 2008: Variational bias correction in ERA-Interim, ECMWF, Technical Memorandum 575, p. 26. Available at: http://www.ecmwf.int/publications/library/do/references/show?id=88715

Dentener, F., Kinne, S., Bond, T., Boucher, O., Cofala, J., Generoso, S., Ginoux, P., Gong, S., Hoelzemann, J. J., Ito, A., Marelli, L., Penner, J. E., Putaud, J.-P., Textor, C., Schulz, M., van der Werf, G. R., and Wilson, J., 2006, Emissions of primary aerosol and precursor gases in the years 2000 and 1750 prescribed data-sets for AeroCom, *Atmos. Chem. Phys.*, 6, 4321-4344, doi:10.5194/acp-6-4321-2006.

Donner, L., B. Wyman, R. Hemler, L. Horowitz, Y. Ming, M. Zhao, J. Golaz, P. Ginoux, S. Lin, M. Schwarzkopf, J. Austin, G. Alaka, W. Cooke, T. Delworth, S. Freidenreich, C. Gordon, S. Griffies, I. Held, W. Hurlin, S. Klein, T. Knutson, A. Langenhorst, H. Lee, Y. Lin, B. Magi, S. Malyshev, P. Milly, V. Naik, M. Nath, R. Pincus, J. Ploshay, V. Ramaswamy, C. Seman, E. Shevliakova, J. Sirutis, W. Stern, R. Stouffer, R. Wilson, M. Winton, A. Wittenberg, and F. Zeng, 2011: The Dynamical Core, Physical Parameterizations, and Basic Simulation Characteristics of the Atmospheric Component AM3 of the GFDL Global Coupled Model CM3. *J. Climate*, 24, 3484-3519, doi: 10.1175/2011JCLI3955.1.

Dubovik, O., B. Holben, T. Eck, A. Smirnov, Y. Kaufman, M. King, D. Tanr, and I. Slutsker, 2002: Variability of Absorption and Optical Properties of Key Aerosol Types Observed in Worldwide Locations. *J. Atmos. Sci.*, 59, 590608, doi: 10.1175/1520-0469(2002)059< 0590 : $VOAAOP$ >2.0.CO;2.

Flemming, J., Benedetti, A., Inness, A., Engelen, R. J., Jones, L., Huijnen, V., Remy, S., Parrington, M., Suttie, M., Bozzo, A., Peuch, V.-H., Akritidis, D., and Katragkou, E.: The CAMS interim Reanalysis of Carbon Monoxide, Ozone and Aerosol for 2003-2015, Atmos. Chem. Phys., 17, 1945-1983, doi:10.5194/acp-17-1945-2017, 2017.

Flemming, J., Huijnen, V., Arteta, J., Bechtold, P., Beljaars, A., Blechschmidt, A.-M., Diamantakis, M., Engelen, R. J., Gaudel, A., Inness, A., Jones, L., Josse, B., Katragkou, E., Marecal, V., Peuch, V.-H., Richter, A., Schultz, M. G., Stein, O., and Tsikerdekis, A., 2015, Tropospheric chemistry in the Integrated Forecasting System of ECMWF, Geosci. Model Dev.,1295 8, 975-1003, doi:10.5194/gmd-8-975-2015.

Fouquart, Y., B. Bonnel, G. Brogniez, J. Buriez, L. Smith, J. Morcrette, and A. Cerf, 1987: Observations of Saharan aerosols: Results of ECLATS field experiment. Part II: Broadband radiative characteristics of the aerosols and vertical radiative flux divergence. J. Climate Appl. Meteor., 26, 38-52.

Guelle, W., M. Schulz, Y. Balkanski, and F. Dentener, 2001: Influence of the source formulation on modeling the atmospheric global distribution of the sea salt aerosol, J. Geophys. Res., 106, 27,509 27,524.

Haywood, J., P. Francis, S. Osborne, M. Glew, N. Loeb, E. Highwood, D. Tanr, G. Myhre, P. Formenti, and E. Hirst, 2003, Radiative properties and direct radiative effect of Saharan dust measured by the C-130 aircraft during SHADE: 1. Solar spectrum, J. Geophys. Res., 108, 8577, doi:10.1029/2002JD002687, D18.

Haywood, J. and Boucher, O.: Estimates of the direct and indirect radiative forcing due to tropospheric aerosols: A review, *Rev.Geophys.*, 38, 513543, 2000

Hess M., Koepke P., and Schult I., 1998, Optical Properties of Aerosols and Clouds: The Software Package OPAC. *Bull. of the Amer. Met. Soc.*, 79, 5, 831-844.

Hogan, R.J. and Bozzo A., 2016, ECRAD: a new radiation scheme for the IFS. *ECMWF Tech. Memo*, 787

Hollingsworth A., R. J. Engelen, A. Benedetti, A. Dethof, J. Flemming, J. W. Kaiser, J-J. Morcrette, A. J. Simmons, C. Textor, O. Boucher, F. Chevallier, P. Rayner, H. Elbern, H. Eskes, C. Granier, V.H. Peuch, L. Rouil, M.G. Schultz and the GEMS consortium, 2008, Toward a Monitoring and Forecasting System For Atmospheric Composition: The GEMS Project. *Bull. of the Amer. Met. Soc.*, doi:http://dx.doi.org/10.1175/2008BAMS2355.1.

Inness, A., Baier, F., Benedetti, A., Bouarar, I., Chabrillat, S., Clark, H., Clerbaux, C., Coheur, P., Engelen, R. J., Errera, Q., Flemming, J., George, M., Granier, C., Hadji-Lazaro, J., Huijnen, V., Hurtmans, D., Jones, L., Kaiser, J. W., Kapsomenakis, J., Lefever, K., Leitão, J., Razinger, M., Richter, A., Schultz, M. G., Simmons, A. J., Suttie, M., Stein, O., Thpaut, J.-N., Thouret, V., Vrekoussis, M., Zerefos, C., and the MACC team: The MACC reanalysis: an 8 yr data set of atmospheric composition, Atmos. Chem. Phys., 13, 4073-4109, doi:10.5194/acp-13-4073-1392 2013, 2013.

Kaiser, J.W., A. Heil, M.O. Andreae, A. Benedetti, N. Chubarova, L. Jones, J.-J.Morcrette, M. Razinger, M.G. Schultz, M. Suttie, and G.R. van der Werf, 2011: Biomass burning emissions estimated with a global fire assimilation system based on observed fire radiative power. Biogeosciences Discuss., 8(4), 7339-7398.

Kinne, S., D. O'Donnel, P. Stier, S. Kloster, K. Zhang, H. Schmidt, S. Rast, M. Giorgetta, T. F. Eck, and B. Stevens, 2013, MAC-v1: A new global aerosol climatology for climate studies, J. Adv. Model. Earth Syst., 5, 704740, doi:10.1002/jame.20035.

Kim, D., Chin, M., Yu, H., Eck, T. F., Sinyuk, A., Smirnov, A., and Holben, B. N., 2011, Dust optical properties over North Africa and Arabian Peninsula derived from the AERONET dataset, *Atmos. Chem. Phys.*, 11, 10733-10741, doi:10.5194/acp-11-10733-2011.

Koepke, P., M. Hess, I. Schult, and E.P. Shettle, 1997: Global Aerosol Data Set, Report No. 243, Max-Planck-Institut fr Meteorologie, Hamburg, ISSN 0937-1060.

Lau, K. M. and Kim, K. M., 2006, Observational relationships between aerosol and Asian monsoon rainfall, and circulation. *Geophys. Res. Lett.* 33, L21810.

Levy, R. C., Remer, L. A., Kleidman, R. G., Mattoo, S., Ichoku, C., Kahn, R., and Eck, T. F., 2010, Global evaluation of the Collection 5 MODIS dark-target aerosol products over land, *Atmos. Chem. Phys.*, 10, 10399-10420, doi:10.5194/acp-10-10399-2010.

Liu, H., R. T. Pinker, and B. N. Holben, 2005, A global view of aerosols from merged transport models, satellite, and ground observations, J. Geophys. Res., 110, D10S15, doi:10.1029/2004JD004695.

Morcrette, J.-J., A. Beljaars, A. Benedetti, L. Jones, and O. Boucher, 2008: Sea-salt and dust aerosols in the ECMWF IFS model , *Geophys. Res. Lett.*, 35, L24813, doi:10.1029/2008GL036041

Morcrette, J.-J., O. Boucher, L. Jones, D. Salmond, P. Bechtold, A. Beljaars, A. Benedetti, A. Boner, J. W. Kaiser, M. Razinger, et al., 2009: Aerosol analysis and forecast in the European Centre for Medium-Range Weather Forecasts Integrated Forecast System. Part 1: Forward modelling, *J. Geophys. Res.-Atmospheres*, 114(D6), D06206, doi:10.1029/2008JD011235.

Morcrette, J.-J., Benedetti A., Ghelli A., Kaiser J.W., Tompkins A.M., 2011, Aerosol-Cloud-Radiation Interactions and their Impact on ECMWF/MACC Forecasts. *ECMWF Tech. Memo*, 660

Mulcahy, J. P., Walters, D. N., Bellouin, N., and Milton, S. F., 2014, Impacts of increasing the aerosol complexity in the Met Office global numerical weather prediction model. *Atmos. Chem. Phys.*, 14, 4749-4778, doi:10.5194/acp-14-4749-2014.

Parrish, D. F., and J. C. Derber, 1992: The National Meteorological Centers spectral statistical-interpolation analysis system, *Mon. Weather Rev.*,120, 1747 1763.

Reale O., Lau K.M., Da Silva A., 2011, Impact of an Interactive Aerosol on the African Easterly Jet in the NASA GEOS-5 Global Forecasting System. *Wea. Forecasting*, 26, 504-519

Reddy M.S., Boucher O., Bellouin N., Schulz M., Balkanski Y., Dufresne J.-L., and Pham M., 2005, Estimates of global multicomponent aerosol optical depth and direct radiative perturbation in the Laboratoire de Meteorologie Dynamique general circulation model. *J. Geophys. Res.-Atmospheres*, 110, D10S16, doi:10.1029/2004JD004757.

Rémy, S., Benedetti, A., Bozzo, A., Haiden, T., Jones, L., Razinger, M., Flemming, J., Engelen, R. J., Peuch, V. H., and Thepaut, J. N., 2015, Feedbacks of dust and boundary layer meteorology during a dust storm in the eastern Mediterranean, *Atmos. Chem. Phys.*, 15, 12909-12933, doi:10.5194/acp-15-12909-2015.

Rodwell, M. J. and Jung, T., 2008, Understanding the local and global impacts of model physics changes: an aerosol example. *Q.J.R. Meteorol. Soc.*, 134: 14791497. doi:10.1002/qj.298

Schulz, M., G. de Leeuw, and Y. Balkanski, 2004: Sea-salt aerosol source functions and emissions, in Emission of Atmospheric Trace Compounds, edited by C. Granier, P. Artaxo, and C. E. Reeves, pp. 333354, Kluwer Acad., Norwell, Mass.

Simmons, A.J., 2010, Monitoring Atmospheric Composition and Climate, *ECMWF Newsletter*, 123, 10-13.

Solomon S., Daniel J.S., Neely R.R. 3rd, Vernier J.P., Dutton E.G., Thomason L.W., 2011, The persistently variable "background" stratospheric aerosol layer and global climate change *Science*, 12;333(6044):866-70. doi: 10.1126/science.

Stier, P., Feichter, J., Kinne, S., Kloster, S., Vignati, E., Wilson, J., Ganzeveld, L., Tegen, I., Werner, M., Balkanski, Y., Schulz, M., Boucher, O., Minikin, A., and Petzold, A.: The aerosol-climate model ECHAM5-HAM, Atmos. Chem. Phys., 5, 11251156, doi:10.5194/acp-5-1125-2005.

Tompkins, A. M., C. Cardinali, J.-J. Morcrette, and M. Rodwell, 2005, Influence of aerosol climatology on forecasts of the African Easterly Jet, *Geophys. Res. Lett.*, 32, L10801, doi:10.1029/2004GL022189.

Tang, I. N., A. C. Tridico, and K. H. Fung, 1997, Thermodynamic and optical properties of sea salt aerosols, J. Geophys. Res., 102, 23,269-23,275.

Tang, I. N., and H. R. Munkelwitz, 1994: Water activities, densities, and refractive indices of aqueous sulfates and sodium nitrate droplets of atmospheric importance. J. Geophys. Res., 99, 18 801-18 808.

Tanré, D., J.-F . Geleyn and J. Slingo, 1984: First results of the introduction of an advanced aerosol-radiation interaction in the ECMWF low resolution global model, in H. Gerber and A. Deepak, eds., *Aerosols and Their Climatic Effects*, A. Deepak Publ. Hampton, Va., pp. 133-177.

Tegen,I., P. Hoorig, M.Chin, I. Fung, D.Jacob, and J. Penner, 1997, Contribution of different aerosol species to the global aerosol extinction optical thickness: Estimates from model results, *J. Geophys. Res.*, 102, 23,895-23,915.

Toll, V., Reis, K., Ots, R., Kaasik, M., Mnnik, A., Prank, M., and Sofiev, M., 2015, SILAM and MACC reanalysis aerosol data used for simulating the aerosol direct radiative effect with the NWP model HARMONIE for summer 2010 wildfire case in Russia, *Atmos. Environ.*, 121, 75-85, doi:10.1016/j.atmosenv.2015.06.007.

Toll, V., Gleeson, E., Nielsen, K. P., Mnnik, A., Maek, J., Rontu, L., and Post, P., 2016, Impacts of the direct radiative effect of aerosols in numerical weather prediction over Europe using the ALADIN-HIRLAM NWP system, *Atmos. Res.*, 172-173, 163-173, doi:10.1016/j.atmosres.2016.01.003.

Toon, O. B., Ackerman, T. P., 1981, Algorithms for the calculation of scattering by stratified spheres. *Applied Optics* 20 (20), 3657-3660. doi:10.1364/ao.20.003657.

Vinoj V., Philip J. Rasch, Hailong Wang, Jin-Ho Yoon, Po-Lun Ma, Kiranmayi Landu and Balwinder Singh, 2014, Short-term modulation of Indian summer monsoon rainfall by West Asian dust. *Nature Geoscience*, 7, 308-313, doi:10.1038/ngeo2107.

Yu, H., M. Chin, D. M. Winker, A. H. Omar, Z. Liu, C. Kittaka, and T. Diehl, 2010, Global view of aerosol vertical distributions from CALIPSO lidar measurements and GOCART simulations: Regional and seasonal variations, *J. Geophys. Res.*, 115, D00H30, doi:10.1029/2009JD013364.

Wang, C., Kim, D., Ekman, A. M. L., Barth, M. C. and Rasch, P. J., 2009, Impact of anthropogenic aerosols on Indian summer monsoon. *Geophys. Res. Lett.* 36, L21704.

Winker, D. M., Tackett, J. L., Getzewich, B. J., Liu, Z., Vaughan, M. A., and Rogers, R. R., 2013, The global 3-D distribution of tropospheric aerosols as characterized by CALIOP, *Atmos. Chem. Phys.*, 13, 3345-3361, doi:10.5194/acp-13-3345-2013.

Wild, M., 2012, Enlightening Global Dimming and Brightening. *Bull. Amer. Meteor. Soc.*, 93, 2737, doi: 10.1175/BAMS-D-11-00074.1.

Wild, M., 2009: Global dimming and brightening: A review. *J. Geophys. Res.*, 114, D00D16, 10.1029/2008JD011470.

Woodward, S., 2001, Modeling the atmospheric life cycle and radiative impact of mineral dust in the Hadley Centre climate model, *J. Geophys. Res.*, 106(D16), 18155-18166, doi:10.1029/2000JD900795.